Purpose-driven polymers: Mechanistic insights and empirical advances in inverse vulcanized polysulfides for mercury remediation

CHEMICAL ENGINEERING JOURNAL

Lawrence A. Limjuco, Jayson S. Garcia, Zhentao Wu, Paul D. Topham, Matthew Derry, Mona Semsarilar, Abed Alaswad

PII: S1385-8947(25)11655-0

DOI: https://doi.org/10.1016/j.cej.2025.170810

Reference: CEJ 170810

To appear in:

Received date: 9 September 2025

Revised date: 8 November 2025

Accepted date: 11 November 2025

Please cite this article as: L.A. Limjuco, J.S. Garcia, Z. Wu, et al., Purpose-driven polymers: Mechanistic insights and empirical advances in inverse vulcanized polysulfides for mercury remediation, (2024), https://doi.org/10.1016/j.cej.2025.170810

This is a PDF of an article that has undergone enhancements after acceptance, such as the addition of a cover page and metadata, and formatting for readability. This version will undergo additional copyediting, typesetting and review before it is published in its final form. As such, this version is no longer the Accepted Manuscript, but it is not yet the definitive Version of Record; we are providing this early version to give early visibility of the article. Please note that Elsevier's sharing policy for the Published Journal Article applies to this version, see: https://www.elsevier.com/about/policies-and-standards/sharing#4-published-journal-article. Please also note that, during the production process, errors may be discovered which could affect the content, and all legal disclaimers that apply to the journal pertain.

Purpose-Driven Polymers: Mechanistic Insights and Empirical Advances in Inverse Vulcanized Polysulfides for Mercury Remediation

Lawrence A. Limjuco^{a,*}, Jayson S. Garcia^b, Zhentao Wu^a, Paul D. Topham^c, Matthew Derry^c, Mona Semsarilar^d, Abed Alaswad^{a,e}

- ^a Energy and Bioproducts Research Institute (EBRI), Aston University, Aston Triangle, Birmingham B4 7ET West Midlands, United Kingdom
- ^b Energy Engineering Program, National Graduate School of Engineering, College of Engineering, University of the Philippines Diliman, Quezon City 1101, Philippines
- ^c Aston Institute for Membrane Excellence (AIME), Aston University, Aston Triangle, Birmingham B4 7ET West Midlands, United Kingdom
- ^d Institut Européen des Membranes IEM UMR 5635, Univ Montpellier, CNRS, ENSCM, 34090 Montpellier, France
- ^e Mechanical, Biomedical and Design, College of Engineering and Physical Science, Aston University, Aston Triangle, Birmingham B4 7ET West Midlands, United Kingdom

Abstract

Inverse vulcanized polysulfides (IV PS) are an emerging class of sulfur-rich polymers that have garnered increasing attention as promising adsorbents for mercury (Hg) remediation. Their chemical tunability, abundance of soft Lewis base sulfur moieties, and alignment with green chemistry principles position them as potentially sustainable and cost-effective solutions for addressing Hg, one of the most toxic and persistent pollutants. This promise is further reinforced by their green credentials: IV PS are synthesized from elemental sulfur, an abundant industrial by-product, often in combination with renewable monomers, enabling sustainable, high-capacity sorbents with low production cost. Yet, a critical question remains: have IV PS truly delivered on their potential as ideal Hg adsorbents? This review explores the purpose-driven development of IV PS-based Hg adsorbents, spanning foundational synthesis strategies to emerging computational approaches. Key motivations discussed include: (1) comonomer selection; (2) enhancement of adsorbent properties (e.g., surface area, wettability, reactivity, and topology); (3) vulcanization advances in inverse strategies (e.g., catalyst-free multicomponent polymerization/nucleophilic activation and catalysis); (4) performance evaluation; and (5) integration of computational tools. Addressing whether IV PS have reached their potential, this review critically examines performance metrics (i.e., adsorption isotherms, kinetics, selectivity, and cost-effectiveness) underscoring the need for standardized performance testing reporting and introduces the concept of percent binding site utilization to better leverage their high sulfur content. By identifying critical gaps in design development and performance evaluation of IV PS, this review provides a foundation for advancing IV PS from promising laboratory materials to practical, scalable solutions for Hg remediation.

Keywords: inverse vulcanization, polysulfides, mercury remediation, adsorption, green chemistry

1. Introduction

Inverse vulcanization (IV) has emerged as a transformative approach to reimagine sulfur's potential. This strategy not only transforms sulfur, long considered a burdensome byproduct of hydrocarbon refining, into valuable materials but also addresses the pressing "sulfur surplus problem" through sustainable polymer innovation.

Sulfur is abundant, available, and cheap. With effectively limitless geological reserves [1], global sulfur production is largely driven as a by-product of fossil fuel processing and is often heavily subsidized, resulting in exceptionally low market prices for downstream industrial users. In fact, production volumes in some years have outpaced global demand [2]. Over the past four decades, the inflation-adjusted price of sulfur has consistently remained below \$40 per metric ton [3], except during periods of geopolitical instability or economic downturns that temporarily disrupt the balance between supply and demand (Figure 1a).

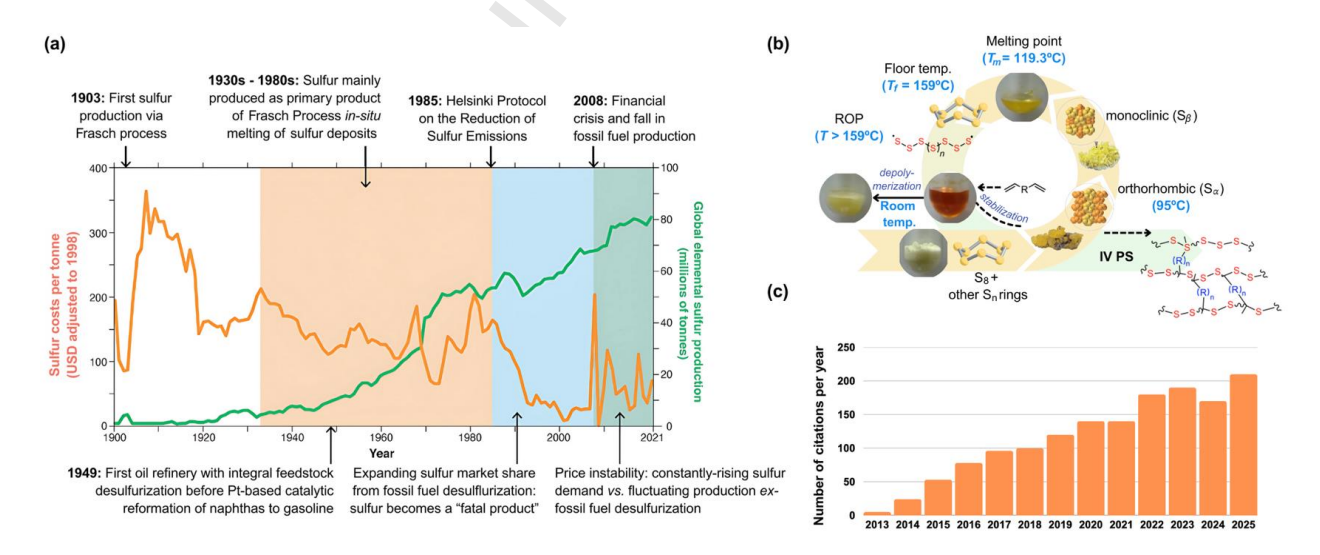


Figure 1. Motivation establishment: a) comparison of sulfur's global supply and cost per tonne corrected to 1998 USD (adapted from Maslin et al., 2021[3]); b) schematic diagram of sulfur

chemistry reflecting inverse vulcanization [4,5]; c) number of citations of pioneering work of Chung et al., 2013[5] on inverse vulcanization (citation data retrieved and updated from Google Scholar up to October 2025).

These motivated the direct utilization of elemental sulfur (S_8) via different copolymerization strategies to modify the properties of S_8 by incorporation into polymeric materials (Table 1). This includes anionic copolymerization with propylene sulfide [4,6], free radical copolymerization of S_8 with styrene [7], copolymerization of diynes with S_8 to form regio-random polythiophenes [8], and copolymerization of cyclic disulfides with S_8 , which afford intractable copolymers with increasing sulfur feed ratios [9]. Although all of these report potential for direct S_8 utilization, these materials either have low degrees of sulfur incorporation into the final copolymer or form polymeric materials with limited processability and tunability of properties [5].

In 2011, Chung's group pioneered the use of S_8 as both reactant and solvent to synthesize sulfurrich copolymers[10] termed *inverse vulcanization* in 2013[5]. At temperature above the sulfur floor temperature ($T_f = 159^{\circ}$ C), the cycloocta-S undergoes homolytic scission initiating the polymerization due to its addition, in propagation, to polysulfur macroradicals [4]. However, this polymeric sulfur is thermodynamically unstable at room temperature [11] leading to depolymerization back to monomeric ring of varying ring size [5]. In inverse vulcanization (IV), the diradical polymeric sulfur is stabilized by quenching with vinylic comonomer, yielding polysulfides with high sulfur content (50–90 wt%) and tunable sulfur rank ($-S_n$ – chains, typically n = 2-8) (Figure 1b). These structural features significantly influence the thermal, mechanical, and chemical properties of the materials. The simplicity, low cost, solvent-free, and high atom economy of the process highlight its potential for scalable sulfur valorization.

Table 1. Elemental sulfur copolymerization strategies.

Title	Reaction	Reference
Anionic copolymerization of elemental sulfur	Solvent: benzene or toluene $ \underline{\text{Ir}} \widehat{CH_3} \widehat{CH_3} $	[4]
Anionic copolymerization of elemental sulfur with 2,2-dimethylthiirane	$\begin{array}{cccccccccccccccccccccccccccccccccccc$	<u> </u> [6]
Chemistry of the modification of sulfur by the use of dicyclopentadiene and of styrene	$\begin{array}{c c} & H_2C - C & + & S_8 & \longrightarrow & C - C - S_x \\ & & & & & CH_3 & & \\ & & & & & & CH_3 & & \\ & & & & & & & \\ & & & & & & & \\ & & & & & & & \\ & & & & & & & \\ & & & & & & & \\ & & & & & & & \\ & & & & & & & \\ & & & & & & & \\ & & & & & & & \\ & & & & & & & \\ & & & & & & & \\ & & & & & & & \\ & & & & & & & \\ & & & & & & & \\ & & & & & & & \\ & & & & & & & \\ & & & & & \\ & & & & & & \\ & & & & & \\ & & & & & & \\ & & & & & \\ & & & & & \\ & & & & & \\ & & & & & \\ & & & & & \\ & & & & & \\ & & & & & \\ & & & & & \\ & & & & \\ & & & & \\ & & & & \\ & & & & \\ & & & & \\ & & & & \\ & & & & \\ & & & & \\ & & & & \\ & & & & \\ & & & & \\ & & & & \\ & & & & \\ & & \\ & & \\ & & & \\ & & \\ & $	[7]
Palladium-catalysed cycloaddition copolymerization of diynes with elemental sulfur to poly(thiopene)s	$R \rightarrow \mathbb{R}$	[8]
Copolymerization of elemental sulfur with cyclic (arylenedisulfide) oligomers	*S ₈	sx) _m [9]

Since its first report in 2013, the IV technique has garnered increasing attention, as reflected by its growing citation record (Figure 1c). This interest is driven by the versatility in producing sulfur-rich polymers with diverse applications including optical materials [12–16], cathodes for Li-S batteries[17–19], controlled release fertilizers[20–22], antimicrobial additives[23,24], and adsorbents for hazardous material remediation[25–28]. The growing body of related patents filed (Table 2) further highlights the broad technological relevance of inverse vulcanized materials.

Among these applications, a particularly compelling and chemically rationalized use is in the adsorption of heavy metals [29], especially mercury (Hg²⁺), a priority pollutant considered by the World Health Organization [30]. Based on Pearson's Hard–Soft Acid–Base (HSAB) theory, sulfur (a soft Lewis base) exhibits a strong affinity toward soft Lewis acids like Hg²⁺ [31]. This rationale, combined with the abundant sulfur-based functional groups in inverse vulcanized polysulfides (IV PS), makes these materials highly suitable for Hg²⁺ capture. This further compounds the green chemistry credentials of IV: utilizing elemental sulfur, an industrial by-

product, and often incorporating renewable monomers, suggesting the potential for sustainable, high-capacity, and cost-effective Hg²⁺ sorbents.

But this raises a critical question: have IV PS truly delivered on their potential as ideal Hg²⁺ adsorbents? This review article aims to answer this question by discussing the mechanistic insights and empirical advances in IV PS for Hg remediation. Mercury cycling in the environment is discussed to establish the practical significance of Hg²⁺ in laboratory-scale evaluation of Hg remediation technologies (SI Section 1). Adsorption, as cost-effective Hg²⁺ remediation technology, was then discussed (SI Section 2), reviewing the concept of HSAB (SI Section 3) as an underlying principle for the design/functionalization of Hg²⁺ adsorbents, i.e., based on S-based functional groups (SI Section 4). This provides a compelling rationale for the design of S-rich materials for Hg²⁺ remediation, rendering the IV PS as ideal Hg²⁺ adsorbents. The different motivations in the development of IV PS-based Hg²⁺ adsorbents, since the first proof of IV PS for Hg²⁺ binding [32], have been comprehensively tracked and discussed. These include (1) selection of comonomer [33-38]; (2) enhancement of characteristics of the IV PSbased Hg²⁺ adsorbent which include morphology (i.e., surface area) and wettability, functionality, reactivity, and topology via multiple component system IV PS [38–45]; (3) improvement of the IV reaction (e.g., catalyst-free multicomponent polymerization [40,46] and nucleophilic activation [47] and catalysis [48]); (4) evaluation of factors affecting performance of IV PS; and more recently, 5) employment of theoretical and computational studies (e.g., machine learning [41] and density functional theory [44]).

Whilst different review papers have been written about IV PS (Table 3), very few papers have focused on metal adsorption at the time of writing: two focused on different target metals, [49,50] whilst one focuses primarily on synthetic modifications aimed at improving uptake ratios

[51]. One paper focused on IV PS as mercury sorbents with special emphasis on increasing surface area to improve mercury uptake and life-cycle management [52]. However, other mercury-binding polymers made from sulfur that do not contain polysulfides were not discussed. Meanwhile, to establish the viability of IV PS as ideal Hg adsorbents, these sulfur-functionalized materials were discussed in this review (SI Section 4). Whilst addressing the research question whether IV PS has delivered its potential as an ideal Hg adsorbent, this review paper also provides insights and clarifications on proper evaluation of performance in terms of adsorption isotherm, kinetics, selectivity, and cost effectivity vis-à-vis adsorption capacity. This review also discusses what mechanistically affects the performance of IV PS-based Hg adsorbents, namely surface area *versus* wettability, which leads to the introduction of a critical performance parameter, percent (%) binding site utilization, to maximize and leverage the high S-content of the IV PS for Hg adsorption.

Table 2. Selected filed patents on inverse vulcanization.*

Patent Number	Title
CN106549157 A	Hollow sphere shape class graphite-phase C ₃ N ₄ and elemental sulfur composite material and its preparation method and application
CN107293694 A	Multi-sulfur polymer composite material, its preparation method and application
CN111019134 A	Preparation method of porous high sulfur polymer for metal recovery
CN112831047 A	Method for preparing sulfur-containing polymer by photocatalytic reverse vulcanization under room temperature conditions
CN113929909 A	Method for preparing sulfur-rich polymers at room temperature by mechanochemically induced reverse vulcanization reaction
CN114682225 A	Method for simultaneous treatment of heavy metal chromium and methyl orange in sewage by using magnetic porous nano-adsorbent
CN114709406 A	Sulfur-rich copolymer material, lithium sulphur battery positive electrode material and preparation method thereof
CN115368567 A	Preparation method of reverse vulcanization copolymer cathode active material and all-solid battery
CN115873185 A	Sulfur-containing polymer and preparation method thereof
CN116581272 A	Cathode material having pentaerythritol-based organic matter for modified lithium-sulfur battery and preparation method and application thereof
CN117186372 A	Sulfur-containing multifunctional polylactic acid material and preparation method thereof
CN117343326 A	Preparation method of industrial-scale reverse vulcanization sulfur-rich polymers through programmed temperature rise
CN117447761 A	Preparation method of sulfur-containing ionic liquid polymer porous membranes through reverse vulcanization reaction for heavy metal ion adsorption
CN117624601 A	Antibacterial toughening agent based on polysulfide for antibacterial super-tough polylactic acid
CN117865340 A	Method for preparing sulfur-rich polymer denitrification biofiller for sewage treatment
CN118022698 A	Method for preparing mercury-removing adsorbent based on reverse-sulfide sulfur-rich copolymer
CN118105959 A	Method for preparing sulfur copolymer adsorbent
CN118497826 A	Method for preparing polysulfide polymer intercalated nickel-molybdenum bimetallic hydroxide composite and use thereof
CN118651846 A	Hard carbon negative electrode material and preparation method and application
CN118962872 A	Method for preparing mid-infrared sulfur-based polymer microlens array in infrared band stereo imaging and

	wavefront measurement
CN119517983 A	Sulfur-rich polymer and preparation method, positive electrode material, positive electrode and lithium-sulfur
	battery thereof
CN119591785 A	Preparation method of sulfur-rich polymer for waterproof coating composition
CN120261570 A	A method for preparing an organic sulfur copolymer electrode material
DE102015115674	Cathode material for lithium-sulfur batteries
A1	
KR1321491 B1	Method for manufacturing sulfur polymer cement and concrete
KR2019010399 A	Nanofiber membrane for mercury adsorption comprising polysulfide prepared by reaction of sulfur and hydrophilic comonomer, its production method and application
KR2023045834 A	Sulfur-containing polymer, manufacturing method thereof, and heat resistance and infrared ray transmission polymer film therewith
KR2023045964 A	Sulfur-containing polymer composition, sulfur-containing polymer, and infrared transmission optical film having elasticity and high heat resistance including the same
KR2024070923 A	Method for producing sulfur copolymers for optical elements with excellent optical property and optical devices
KR2025092514 A	Method for producing sulfur-containing polymer by inverse vulcanization polymerization and vacuum heat treatment
MA63492 A1	Preparation of mesoporous materials containing polysulfides and their use
US20140199592 A1	High sulfur content copolymers and composite materials and electrochemical cells and optical elements using them
US20180079865 A1	Cathode composite materials for lithium sulfur (Li-S) batteries
US20180100037 A1	Copolymerization of elemental sulfur and epoxy functional styrenics
US20180105649	Three-dimensional printing of ultra-high refractive index polymers prepared from sulfur-, selenium-, and
A1	chalcogenide-containing monomers and organic comonomers
US20190338076	Fire retardant compositions utilizing elemental sulfur
A1	
US20200346196	Catalysts for making polymeric materials from elemental sulfur, and the method of using the same
A1	
US20230089692	Dynamic covalent polymerizations with elemental sulfur and sulfur prepolymers

A1	
US20230242820	Copolymerization of sulfur with bio-oil or biomass monomers
A1	
US20230331940	Chalcogenide hybrid inorganic/organic polymer (CHIP) materials as improved crosslinking agents for
A1	vulcanization
US20240097182	High energy solid-state batteries and methods of making the same
A1	
US20250326895	Biogenic catalysts for sulfur polymerization
A1	
US9567439 B1	Sulfur composites and polymeric materials from elemental sulfur
WO2013023216 A1	High sulfur content copolymers and composite materials and electrochemical cells and optical elements using
	high sulfur content copolymers
WO2016064615 A1	Sulfur-limonene polysulfide for sequestering palladium and mercury from aqueous solution
WO2017004186 A1	Methods of utilizing elemental sulfur for flame retardant polymers and additives
WO2017011533 A1	Copolymerization of elemental sulfur to synthesize high sulfur content polymeric materials
WO2017027739 A1	Copolymerization of elemental sulfur and thiocarbonyl-containing compounds
WO2017181217 A1	Metal adsorbent material and uses of polymeric polysulfide
WO2018026493 A1	Dynamic covalent polymerizations with elemental sulfur and sulfur prepolymers
WO2018183702 A1	Chalcogenide hybrid inorganic/organic polymers (CHIPs) for photonic crystal materials and devices
WO2018232155 A1	Chalcogenide hybrid inorganic/organic polymer materials as improved crosslinking agents for vulcanization
WO2019012278 A1	Sulfur-doped carbonaceous porous materials
WO2019012278 A1	Sulfur polymers and compositions and their use as an active electrode material
WO2019008182 A1	Sorbent compositions
WO2020070407 A1	Chalcogenide hybrid organic/inorganic polymers films and coatings and the use thereof
WO2020072703 A2	Photoresponsive chalcogenide hybrid organic/inorganic polymer films having high refractive index and mid-IR
11 02020012103 A2	transparency suitable for use in waveguides
WO2020191340 A1	Chalcogenide hybrid organic/inorganic polymers and methods for producing and using the same
WO2020198778 A1	Materials and processes for recovering precious metals
WO2020198778 A1	Methods for processing polysulfide polymers
11 02021201103 A1	memous for processing porysumue porymers

WO2022217023 A1	Refractive index contrast polymers and methods for producing and using the same
WO2022239780 A1	Sulfur-containing compound and high molecular weight material
WO2023150825 A1	New polymers and uses thereof
WO2023214184 A1	Nanoparticles comprising inverse vulcanized sulfur polymer, water filtration membrane, and method for
	removing heavy metals from liquids
WO2023225615 A1	Methods for continuous production of sulfur polymer cement
WO2025118407 A1	Method for preparing industrial-scale inverse-vulcanized sulfur-rich polymer by means of temperature
	programming

^{*} Patent search via CAS SciFinder for "inverse vulcanization", "reverse vulcanization", "sulfur polymer", and inventor-assisted queries (regardless of the status: approved, rejected, or abandoned). All items in every keyword search were checked to ensure relevant or related to the IV PS. Not exhaustive.

^{*} This table highlights patented applications and compositions rather than academic variations of inverse vulcanization chemistry, which are discussed in Section 3.3.

A standardized nomenclature for sulfur-containing products from IV has yet to be established. In the Li–S battery literature, the term "polysulfides" typically refers to inorganic salts composed of multi-sulfide anions $(S_x^{2-}, x \ge 2)$ [53]. In contrast, within the context of IV, "polysulfides" has been used to describe polymers consisting of polysulfur chains crosslinked by organic moieties [54–56]. These materials have also been referred to as "inverse vulcanized polymers," [57] "organic polysulfanes," [58] "chalcogenide hybrid inorganic/organic polymers (CHIPs)," [59] or simply "sulfur polymers." [60,61] In this work, the term "IV PS" is adopted. For consistency, products are denoted as poly(S-comonomer) to describe the materials obtained from the one-pot, solventless, direct reaction of sulfur with a comonomer, unless specified otherwise.

Table 3. Summary of review papers on inverse vulcanization.

Review title	Content	Ref.
Recent approaches for the direct use of elemental sulfur in the synthesis and processing of advanced materials	 Physical processing of elemental sulfur Chemical modification of elemental sulfur 	[62]
Polymerizations with elemental sulfur: A novel route to high sulfur content polymers for sustainability, energy and defense	 Elemental sulfur production and consumption High sulfur-content materials Challenges in sulfur chemistry and processing Sulfur as an unconventional solvent and reaction medium Useful properties and modern applications of high S-content polymeric materials 	[63]
Green chemistry and polymers made from sulfur	 Sulfur as a widely available and underused building block Polymers and materials made from sulfur Polysulfides for environmental protection and remediation Polysulfides for sustainable energy production and storage 	[64]
Sulfur chemistry in polymer and materials science	 Synthesis of sulfur functional groups Applications of sulfur in polymer and materials science 	[65]

Synthesis and applications of polymers made by inverse vulcanization	Synthesis of polymers by inverse vulcanization	[66]
	Applications of polymers prepared by inverse vulcanization	
Copolymerization of vegetable oils and bio-based	 Bio-based polymers 	[67]
monomers with elemental sulfur: A new promising	 Vegetable oils for the development of 	
route for bio-based polymers	bio-based polymers	
	Sulfur-based polymers	
	Bio-based polymers by	
	copolymerization of vegetable oils with sulfur	
	 Bio-based polymers by 	
	copolymerization of bio-derived	
	monomers with sulfur	
Sustainable applications utilizing sulfur, a by-product	 Sulfur applications in the fertilizer 	[2]
from oil and gas industry: A state-of-the-art review	industry	
	 Sulfur as additive in construction 	
	materials	
	 Sulfur as feedstock for polymers 	
	 Sulfur in batteries 	
	 Sulfur (with additives) as a heat 	
	transfer fluid and storage medium	
Polymers Made by Inverse Vulcanization for Use as	 Sulfur Polymers by Inverse 	[52]
Mercury Sorbents	Vulcanization	
	 Sulfur Polymers as Mercury Sorbents 	
	 Increasing Surface Area to Improve 	
	Mercury Uptake	
	 Crosslinker Considerations 	
	 Sorption of Different Forms of 	
	Mercury	
	Life-Cycle Management	
Evaluation of properties of sulfur-based polymers	Recent advances in sulfur	[68]
obtained by inverse vulcanization: Techniques and	polymerization by inverse	
challenges	vulcanization	
	• Characterization of inverse vulcanized	
Synthesis and applications of inverse vulcanized	copolymers	[60]
Synthesis and applications of inverse vulcanized polysulfides from bio-crosslinkers	Vegetable oils and plant extracts as crosslinker	[69]
	• The chemistry between elemental	
	sulfur and the bio-crosslinkers	
	Applications of polysulfides	
Delementation with Element 1 C-1C-1C	synthesized from bio-crosslinkers	[70]
Polymerizations with Elemental Sulfur: From	Origins of sulfur from petroleum	[70]
Petroleum Refining to Polymeric Materials	refining	
	 Liquid sulfur as a new reaction medium 	
	Inverse vulcanization	
	 Cathodes for Li-S batteries 	
	Cathodes for Li-S batteriesHigh refractive index polymers for	
	- Then remactive index polymers for	

	 infrared optics Functionalization and post-polymerization modifications Emerging fields of use for S-derived polymers 	
On the fundamental polymer chemistry of inverse vulcanization for statistical and segmented copolymers from elemental sulfur	 Homolytic S₈ ring-opening polymerization Inverse vulcanization: Copolymerization in liquid sulfur Classical prepolymer approaches to segmented copolymers Segmented polyurethane copolymers from elemental sulfur Flame retardant properties of sulfurderived polymers 	[71]
A review on use of elemental sulphur in the synthesis of sulphur-based polymers	 Sulfur co-polymer thermal and rheological characteristics Melt processing of sulfur copolymers into micropatterned films Inverse vulcanization with natural olefinic comonomers Application of inverse vulcanization in LiS batteries 	[72]
Polysulfides as sorbents in support of sustainable recycling	 Inverse vulcanized polysulfides Polysulfides as selective metal/ion sorbents Polysulfides and activated carbon composite materials Scale up potential and end of life 	[50]
Inverse vulcanized polymers for sustainable metal remediation	 Metal remediation Post remediation 	[49]
The recent development of inverse vulcanized polysulfide as an alternative adsorbent for heavy metal removal in wastewater	 Polysulfide adsorbent via inverse vulcanization Effect of important factors for removal process Adsorption mechanism 	[51]
Green and sustainable natural derived polysulfides for a broad range of applications	Fabrication of polysulfidesNatural product derived polysulfides	[73]
Sulfur Polymer as Emerging Advanced Materials: Synthesis and Applications	 Polysulfides through polycondensation Inverse vulcanization principle Supramolecular polysulfide polymers Processing techniques to expand applicability 	[74]

A Comprehensive Exploration of Polysulfides, From Synthesis Techniques to Diverse Applications and Future Frontiers	 Polysulfide preparation techniques Comparison and advantages and disadvantages of polymerization techniques 	[75]						
	 Comparison, uniqueness, and limitations of polysulfide applications Scope of modeling, simulations, and artificial intelligence in the field of 							
Inverse vulcenisation: a new Starter's guide to an	polysulfides	[76]						
Inverse vulcanisation: a new Starter's guide to an emerging field	 Origin, applications, and alternative synthetic routes of inverse vulcanization 	[/0]						
	 Characterization methods, post- synthetic modification, and mechanistic considerations 							
A Decade Development of Inverse Vulcanization Towards Green and Sustainable Practices	 Synthesis and post-modification of polysulfides 	[77]						
	 Properties of the polysulfides synthesized by inverse vulcanization 							
	Alternative renewable resources for inverse vulcanization							
	Applications of the polysulfides derived from renewable resources							
Adding Value into Elementary Sulfur for Sustainable	Emerging polysulfide libraries	[11]						
Materials	 Applications of sulfur-based copolymers 							
A critical review on the sustainability of inverse vulcanised polymers	The lifecycle of inverse vulcanized materials	[78]						
	 Production phase: technical and economic challenges 							
	 Use phase: applications and ageing of IV materials 							
	 System sustainability 							
	• End-of-life							
	Measuring sustainability Cycleding for future life available.							
	 Guideline for future life-cycle assessments 	[77]						
	 Key issues in ecological assessment of 							
	polymers							
	 Framework and methodological 							
2. Inverse vulcanized polysulfides as ideal sulfu	decisions							

2. Inverse vulcanized polysulfides as ideal sulfur-rich Hg adsorbent

Rationalized from the classical reaction between sulfur and terpenes [79–81], the first IV PS tested for Hg²⁺-binding properties utilized D-limonene, a renewable monomer from the citrus industry [32]. The equal-mass sulfur-limonene oligomeric polysulfide effectively demonstrated

binding with Hg²⁺: 55% removal from aqueous solution, Hg²⁺-selective chromogenic response to detect mercury from water and Hg²⁺-spiked river samples, and binding with Hg²⁺ present in mud or soil suspensions [32]. This pioneering work initiated the development of IV PS for mercury remediation (Table 4 and SI Table S6).

Anchored in HSAB theory (SI Section 3) as the underlying rationale, the development of IV PS for mercury remediation has been guided by diverse practical motivations and theoretical insights: (1) choice of comonomer [33–38]; (2) characteristics of the IV PS-based Hg²⁺ adsorbent which include enhancements of morphology (i.e., surface area) and engineering of wettability, functionality, reactivity, and topology via multiple component system IV PS [38–45]; (3) improvement of the IV reaction (e.g., catalyst-free multicomponent polymerization [40,46] and nucleophilic activation [47] and catalysis [48]; (4) factors affecting performance of IV PS; and more recently, (5) theoretical and computational studies, such as machine learning [41], density functional theory [44] and computational fluid dynamics [82].

Table 4. Inverse vulcanized polysulfides for Hg remediation. Journal Pre-proof

								PERFO	DRMANCE 1	EVALUATIO	N						
				Feed Cha	racteristic			Adsorption isothern	n	Kin	etics		Selectivity			Recycla	ability
Entr y	Material*	Ref ·	Feed matrix	Hg speciation (salt)	C _o (mg/L)	p H	Solid- to- liquid ratio	Adsorption isotherm	Ads. Cap. (q, mg/L)	Total adsorptio n / equilibriu m time	Kinetics constant	Competi ng cations	K_d	Separ a-tion factor (\alpha)	Concentr a-tion factor (CF, L/g)	Strippi ng Sol'n	ability Eff. (cycle s) -
1	Poly(S-DIB)	[83]	DI water	(Hg ²⁺) HgCl ₂	2 mg/L		100 mg / 5 mL	-	0.1	3 hrs	-		-	-	-	-	-
2	Poly(S-DIB)/ PMMA nanofiber	[84	DI water	(Hg ²⁺) HgCl ₂	600 mg/L	5	20 mg/ 20 mL	P	440	< 5 mins		% removal: Cd ²⁺ (12.9%), Co ²⁺ (12.5%), Zn ²⁺ 16.5%), Pb ²⁺ (13.6%), Cu ²⁺ (12.2%), Fe ³⁺ (18.9%), Hg ²⁺ (93.3%) 10mL of a 0.7mM; 10mg PS	2710 ml/g	-	-	-	-
3	Porous carbon doped with poly(S-DCPD)	[85]	DI water	(Hg ²⁺) HgCl ₂	20- 1000 mg/L	3-4	15, 30, 60 mg/ 12 mL	Langmuir	850	1 hr	-	% metal salt removed from individual salt solution: Fe ³⁺ (~10%), Co ²⁺ (<5%), Cr ³⁺ (<5%), Cu ³⁺ (<5%)), Hg ²⁺ (<5%)), Mn ²⁺ (<10%), Ni ²⁺ (<3%) Me ⁿ⁺ (100 ppm), 12 mL, 1 hour, 30 mg PS	58000 mL/g	-	-	-	-

4	Foamed poly(S-DIB)	[33	DI water	(Hg ²⁺) HgCl ₂	2 mg/L	-	5 mL / 100 mg	Journal Pre-	pr _{0.1} of	3 hrs	-	-	328 ml/g	-	-	-	-
5	Foamed poly(S- myrcene)	[33	DI water	(Hg ²⁺) HgCl ₂	2 mg/L	-	5 mL / 100 mg	-	0.1	3 hrs	-	-	1950 ml/g	-	-	-	-
6	Foamed poly(S-farnesol)	[33	DI water	(Hg ²⁺) HgCl ₂	2 mg/L	-	5 mL / 100 mg	-	0.1	3 hrs	-	-	950 ml/g	-	-	-	-
			DI water	(Hg ²⁺) HgCl ₂ Hg ⁰ (Hg ²⁺) Hg(NO ₃) ₂	3.5 mg/L 74 mM 100 mg Hg ⁰		Hg ²⁺ 2 g / 5 mL 8 g / 5 mL Hg ⁰ : 1 g / 100 mg	-	C _o = 3.5ppm (90% rem.) 74mM (91% Hg ²⁺ removal) 99% Hg ⁰ removal	24 hrs	0	-		-	-	-	-
7	Poly(S-canola oil)	[86]	NOM- free control: 10 mM NaPO4 Hg- NOM: Suwann ee River aquatic natural organic matter	Hg-NOM	0.2 - 16 μg/L	8	100 mg / 30 mL	Hg-NOM: Langmuir	Hg(NO ₃) 2:>90% Hg ²⁺ removal. Hg- NOM: fxnl groups on NOM compete with PS: 81% removal. $q_m = 1.11$ $\mu g/g$	48 hrs							
8	Poly(S-DVB)	[35]	Nitroge n (at 40C and 60C)	${ m Hg}^0$	3		50 mg [Hg ⁰ gas]	-	40°C: SSD-7- 3-0.75 (33 μg/g) 60°C: SSD-7- 3-0.75 (151 μg/g)	-	-	-	-	-	-	-	-
9	Poly(S-PA)	[34	DI water	(Hg ²⁺) HgCl ₂ (MeHgCl) Methylmercu ry	2.5, 5, 10, 20, 40 mg/L 2.5 mg/L		600 mg/ 12 mL	-	HgCl ₂ : 90% removal (at C_o = 2.5 ppm) MeHgCl : 30% removal (at C_o = 2.5 ppm)	1 hr	-	-		-	٠	-	-

								Journal Pre-	HgCl ₂ :								
10	Poly(S-squalene)	[34	DI water	(Hg ²⁺) HgCl ₂ (MeHgCl) Methylmercu ry	2.5, 5, 10, 20, 40 mg/L 2.5 mg/L		600 mg/ 12 mL	-	removal (at $C_o =$ 2.5 ppm) MeHgCl: 30%. removal (at $C_o =$ 2.5 ppm)	1 hr	-	-		-	-	-	-
11	Poly(S-DIB)- coated PVA- PAA nanofibrillar films	[87]	DI water	(Hg ²⁺) HgCl ₂	50 mg/L		60 mg (volume not indicate d)	-	26	10 min	-	-	-	-	-	-	-
12	Poly(S-MA-St)	[88	DI water	(Hg ²⁺) HgCl ₂	2.240 mg/L			-	50.5	3 hrs	-	-		-	-	-	-
13	Foamed poly(S-MA-St)	[88]	DI water	(Hg ²⁺) HgCl ₂	2.240 mg/L		100 mg / 5 mL	-	52	3 hrs		-		-	-	-	-
14	Poly(S-DCPD)	[89]	DI water	(Hg ²⁺) HgCl ₂	not indicat ed		not indicate d	Langmuir	2.27	48 hrs	-	-	-	-	-	-	-
15	Poly(S-CEA) (2:1)	[36]	DI water	(Hg ²⁺) HgCl ₂	100- 1000 mg/L	6	25 mg / 50 mL	Langmuir	835	2.5 hrs	-	-	15309 mL/g	-	-	-	-
16	Poly(S-CEA) (1:1)	[36]	DI water	(Hg ²⁺) HgCl ₂	100- 1000 mg/L	6	25 mg / 50 mL	Langmuir	803	2.5 hrs	-	-	4612 mL/g	-	-	-	-
17	Poly(S-CEA) (1:2)	[36]	DI water	(Hg ²⁺) HgCl ₂	100- 1000 mg/L	6	25 mg / 50 mL	Langmuir	634	2.5 hrs	-	-	1751 mL/g	-	-	-	-
18	Poly(S-CEA) (2:1)/PAN MF (150 wt% PS) at 60°C	[36]	DI water	(Hg ²⁺) HgCl ₂	100- 800 mg/L	6	40 mg/ 50 mL	Langmuir	612	2.5 hrs	-	-		-	-	-	-
19	Poly(S-CEA) (2:1)/PAN MF (150 wt% PS) at 50°C	[36]	DI water	(Hg ²⁺) HgCl ₂	100- 800 mg/L	6	40 mg/ 50 mL	Langmuir	591	2.5 hrs	-	-		-	-	-	-
20	Poly(S-CEA) (2:1)/PAN MF (150 wt% PS) at 40°C	[36	DI water	(Hg ²⁺) HgCl ₂	100- 800 mg/L	6	40 mg/ 50 mL	Langmuir	526	2.5 hrs	-	-		-	-	-	-
21	Poly(S-CEA) (2:1)/PAN MF (150 wt% PS) at 30°C	[36	DI water	(Hg ²⁺) HgCl ₂	100- 800 mg/L	6	40 mg/ 50 mL	Langmuir	473	2.5 hrs	PSO: 2.25x10 ⁻⁴ g/mg-min (C _o =200 mg/L) 2.55x10 ⁻⁴ g/mg-min (C _o =800 mg/L)	$\begin{array}{c} Cr^{2+},\\ Cu^{2+},\\ Cu^{2+},\\ Zn^{2+},\\ Pb^{2+},\\ Ni^{2+},\\ Cd^{2+} \end{array}$	Hg ²⁺ 116720 4 L/g	Cr ²⁺ (1125) Cu ²⁺ (5589) Zn ²⁺ (4570) Pb ²⁺ (1433) Ni ²⁺ (10430) Cd ²⁺	Hg ²⁺ (1074) Cr ²⁺ (528) Cu ²⁺ (175) Zn ²⁺ (206) Pb ²⁺ (464) Ni ²⁺ (101) Cd ²⁺ (15)	6M HCl	>95% (5)

								Journal Pre-	proof					(74628			
22	Poly(S-CEA) (6:1)	[37]	DI water	$(Hg^{2+}) HgCl_2$ Hg^0 water Hg^0 soil	300- 1500 mg/L	6	32 mg/ 40 mL	Langmuir	Hg ²⁺ = 989 Hg ⁰ water = 308.6	4 hrs	PSO: 2.39x10 ⁻⁴ g/mg-min (C _o =300 mg/L)	Simulated chloralkal i WW: Hg, Pb, Cd, Mg, Na Actual river sample (ARS)	SCW W: Hg 26095 mL/g ARS: 89542 mL/g	SCW W: Hg/Pb (164) Hg/Cd (897) Hg/Mg (372) Hg/Na (73243) ARS: too many	SCWW: Hg (1193x10 ⁻³) Pb (142x10 ⁻³) Cd (28x10 ⁻³) Mg (66x10 ⁻³) Na (3.6x10 ⁻⁴) ARS: too many	-	-
23	Poly(S-CEA) (6:1)/agar MB (50 wt %) at 30°C	[37	DI water	(Hg ²⁺) HgCl ₂	300- 1500 mg/L	6	32 mg/ 40 mL	Langmuir	437	4 hrs	PSO: 0.16x10 ⁻⁴ g/mg-min (C _o =300 mg/L)	-	-	-	-	-	-
24	Poly(S-CEA) (6:1)/agar MB (100 wt %) at 30°C	[37	DI water	(Hg ²⁺) HgCl ₂	300- 1500 mg/L	6	32 mg/ 40 mL	Langmuir	483	4 hrs	PSO: 0.91x10 ⁻⁴ g/mg-min (C _o =300 mg/L)	-	-	-	•	-	-
25	Poly(S-CEA) (6:1)/agar MB (150 wt %) at 30°C	[37]	DI water	(Hg ²⁺) HgCl ₂ Hg ⁰ water Hg ⁰ soil	300- 1500 mg/L	6	32 mg/ 40 mL	Langmuir	Hg ²⁺ = 527 Hg ⁰ water = 415	4 hrs	PSO: 1.38x10 ⁻⁴ g/mg-min (C _o =300 mg/L)	Simulated chloralkal i WW: Hg, Pb, Cd, Mg, Na Actual river sample (ARS)	SCW W: Hg 4492 mL/g ARS: 82950 mL/g	SCW W: Hg/Pb (49) Hg/Cd (34) Hg/Mg (14) Hg/Na (810) ARS: too many	SCWW: Hg (978x10 ⁻³) Pb (86x10 ⁻³) Cd (118x10 ⁻³) Mg (262x10 ⁻³) Na (6x10 ⁻³) ARS: too many	0.5M HCl/1M thiourea	>99% (5)
26	Poly(S-r-canola)	[90]	DI water	(Hg ²⁺) HgCl ₂ (MEMC) 2- methoxymet hyl mercury chloride	HgCl ₂ : 107 mg/L MEMC : 130 mg/L		1 g / 20 mL	Freundlich	Hg ²⁺ = 8.99 MEMC = 2.01	24 hrs	PSO: HgCl ₂ : 5.77 g/mg-h MEMC: 3.34 g/mg-h	-	Hg ²⁺ : 310 ml/g MEMC : ~100 ml/g	-	-	-	-

27	Poly(S-r-rice bran)	[90	DI water	(Hg ²⁺) HgCl ₂ (MEMC) 2- methoxymet hyl mercury chloride	HgCl ₂ : 107 mg/L MEMC : 130 mg/L		1 g / 20 mL	Journal Pre-	Hg ²⁺ = 10.99 MEMC = 1.97	24 hrs	PSO: HgCl ₂ : 8.42 g/mg-h MEMC: 0.17 g/mg-h	-	Hg ²⁺ : 140000 ml/g MEMC : ~100 ml/g		-	-	-
28	Poly(S-r-castor)	[90	DI water	(Hg ²⁺) HgCl ₂ (MEMC) 2- methoxymet hyl mercury chloride	HgCl ₂ : 107 mg/L MEMC : 130 mg/L		1 g / 20 mL	Freundlich	$Hg^{2+} = 8.15$ MEMC = 2.31	24 hrs	PSO: HgCl2: 58.32 g/mg-h MEMC: 0.65 g/mg-h	-	Hg ²⁺ : 560 ml/g MEMC : 1200 ml/g	-	-	-	-
29	Polyethylenimi ne grafted with poly(S-DEB)	[40]	DI water	(Hg ²⁺) HgCl ₂	200- 2000 mg/L	5	10 mg/ 10 mL	Langmuir-Freundlich	1162	3 hrs	(C _o =2000 mg/L) PSO: k ₂ = 3x10 ⁻⁴ g/mg-min)	-	0.0016 L/mg (from ads. Iso).	-	-	2M HNO ₃	80% (5)
30	Poly(S-DVB)	[91]	DI water	Hg2+	2-10 mg/L		Ads. Iso.: 0.1 g / L Kinetics: 2 mg / L	Langmuir	PSSD: 371.33 µg/g NaSD: 231.28 µg/g	~250 min	PSO: PSSD: 1.32x10 ⁻³ g/μg-min NaSD: 9.52x10 ⁻⁴ g/μg-min	-		-	-	-	-
31	Poly(S-cotton seed oil (SCO) modified by 2- aminoethyl methacrylate (AEMA)	[39	DI water	(Hg ²⁺) HgCl ₂	50- 1600 mg/L	7	30 mg / 10 mL	Langmuir-Freundlich	343.3	10 hrs	PSO: 0.01454/h	-		-	-	2M HNO ₃	>80% (5)
32	Hypercrosslink ed poly(S- styrene)	[92	DI water	(Hg ²⁺) HgCl ₂ (Me-Hg) Methylmercu ry chloride	HgCl ₂ : not indicat ed Me- Hg: 11.45 mg/L	C	20 mg (volume not indicate d)	HgCl2: Langmuir	Hg ²⁺ = 215.9 mg/g mg/g Me-Hg: >99% removal	24 hrs	-	Me (<i>C_o</i> , % rem.): Be (2.4, <1%) Ni (1113, <1%) As (215.4, <1%) Cd (394.4, <1%) Co (797.7, <1%) Mn (1029, <3%) Cr (303.3, <3%) Pb	0.48 (from ads. iso.)			-	-

								Journal Pre-	proof			(219.2, <5%)					
												Se (107.9, ~10%) Ti (4.4, ~40%) Sb (0.4, ~90%) Hg (8.7, >99%)					
33	Poly(S-DCPD-GOB)	[93]	DI water	(Hg ²⁺) HgCl ₂	2 mgL 20 mg/L		50 mg / 10 mL	-	2 mg/L: 100% removal 20 mg/L: 28.8% removal	24 hrs	O,	-		-	-	-	-
34	Magnetic poly(S- DCPD)-doped carbons	[94]	DI water	(Hg ²⁺) HgCl ₂	6.25, 12.5, 25, 50, 100, 250, 500 , 1000 mg/L		20 mg / 10 mL	Langmuir	187.4	~250 mins	PSO: 0.0118 g/mg-min	Me [from, to (ppb)] Cr (296, 283) Mn (1027, 1054) Ni (1012, 1032) Co (746, 756) As (203, 45) Se (83, -) Cd (325, 328) Hg (6, -) Pb (227, 127)	0.01 L/mg			1M thiourea / 0.5M HCl	
35	Sulfur crosslinked poly(m- aminothiophen ol) / potato starch on mesoporous silica	[95]	DI water	(Hg ²⁺) Hg(NO ₃) ₂	50-300 mg/L	5	20 mg / 50 mL	Langmuir	436.68	450 min	PSO: 0.0003 g/mg-min	$K^+, Mg^{2+}, Ca^{2+}, Al^{3+}, Ca^{2+}, Al^{3+}, Cu^{2+}, Ni^{2+}, Zn^{2+}, Pb^{2+}$ Binary system: (i.e., Hg w/ each of those cations).	0.20/mi n (from ads. iso.)	-		0.1M HNO ₃ / 0.1M thiourea	~80% (5)
36	Poly(S- oleylamine - potato starch	[45]	DI water	(Hg ²⁺) Hg(NO ₃) ₂	100- 350 mg/L	4	0.02 g / 50 mL	Langmuir	565.21	5.5 hrs	PSO: 0.0036 g/mg-min	Tested Hg ads. cap. in binary	0.0036 L/mg (from ads.			2M HCl/1M Thioure a	93% (5)

								Journal Pre-	proof			system: Mg ²⁺ .	iso.)				
												system: Mg ²⁺ , Zn ²⁺ , Ca ²⁺ , Ni ²⁺ , Pb ²⁺ , Al ²⁺ , Cu ²⁺					
37	Poly(S- cardanol - potato starch)	[44	DI water	(Hg ²⁺) Hg(NO ₃) ₂	100- 350 mg/L	4	20 mg / 50 mL	Langmuir	618.43	3.5 hrs	PSO: 0.0123 g/mg-min)	Tested Hg ads. cap. in binary system: Mg^{2+} , Zn^{2+} , Ca^{2+} , Ni^{2+} , Pb^{2+} , Al^{2+} , Cu^{2+}	0.0073 L/mg (from ads. iso.)			not indicate d	90% (5)
38	Poly(S-Sty)	[96]	DI water	HgCl ₂ Me-Hg	100 mg/L		20 mg / 10 mL	-	Me-Hg = 47.47 mg/g (S-S- Ti10 UV)	24 hrs	-	-	-	-	-	-	-
39	Poly(S-olive oil)	[97	DI water	(Hg ²⁺) HgCl ₂	100 mg/L	6	350 mg (volume not indicate	Langmuir	130.23	2 hrs	PFO: 2.27/h PSO: 0.14/h	$Na^{+}, K^{+}, Ca^{2+}, Mg^{2+}, Cu^{2+}, Zn^{2+}, Cd^{2+}, Hg^{2+} (100\% removal)$ all other $M^{n+}: <3\%$ removal	ads iso: 2.8x10 ⁻³ L/mg	-	-	-	-
40	Poly(S- soybean oil)	[97]	DI water	(Hg ²⁺) HgCl ₂	100 mg/L	6	d)	Freundlich	42.72	8 hrs	PFO: 0.48/h PSO: 0.01/h	-	ads iso: 1.3x10 ⁻² L/mg	-	•	-	-
41	Poly(S- coconut oil)	[97]	DI water	(Hg ²⁺) HgCl ₂	100 mg/L	6		Langmuir	28.08	6 hrs	PFO: 0.64/h PSO: 0.03/h	-	ads iso: 2.1x10 ⁻² L/mg	-	-	-	-
42	Poly(S- nucleophile - PVC)	[47	DI water	(Hg ²⁺) HgSO ₄	50 mg/L	3	30 mg / 20 mL	Langmuir	309	2 hrs	PSO	% removal:. Ca ²⁺ (-6%), Mg ²⁺ (~5%), Na ⁺ (~3%), K ⁺ (~3%), Hg ²⁺ (~63%).	-	-		-	-

43	Amine @ poly(S-methacrylic acid)	[38	DI water	(Hg ²⁺) HgCl ₂	10-50 mg/L	6	0.05 g / 50 mL	Journal Pre- Redlich-Peterson	proof 44.7	~ 270min	PSO: 0.00203/m in	-	ads. iso: 1.46 L/mg	-	-	6M HCl	>99% (6)
44	Poly(S- AVImCl)	[98	DI water	(Hg ²⁺) HgCl ₂	12.5 to 2000 mg/L	7	2 mL of polymer / 2 mL	-	436	24 hrs		% removal: Hg ²⁺ (88.92%) Au ⁺ (62.73%) Mn ²⁺ (0.47%) As ³⁺ (0%) Co ²⁺ (2.14%) Ni ²⁺ (8.73%) Cr ³⁺ (11.71%)			-	-	-
45	Poly(S-Tha- Cy)	[42]	DI water	$(Hg^{2\uparrow})$ $Hg(NO_3)_2$	200 mg/L	4- 8	1 g/L	Langmuir	129,44	30 sec	Hg ²⁺ : 19.73/min Pb ²⁺ : 0.47/min Cd ²⁺ : 0.61/min Zn ²⁺ : 0.39/min Cu ²⁺ : 0.35/min			•	-	-	80.6% (5)
46	Poly(S- VBC)@ NMDG_KOH _C:	[43]	DI water	(Hg ²⁺) HgCl ₂	10-500 mg/L	6	not indicate d	Langmuir Copoly(SVBC)@NMDG_K OH_C	572.4	210 mins	PSO: 2.24/min	-	.7	-	-	6M HCl	>99% (5)

^{*} IV PS reported as poly(sulfur-comonomer) [poly(S-comonomer)] for consistency. Additional information on synthesis, properties, and processing can be found at Table S6.

3. Motivations for IV PS development in Hg remediation

3.1. Choice of comonomer

Since the seminal work on poly(S-limonene), the development of IV PS, especially for Hg²⁺ remediation, has been mainly motivated on enhancing the green credentials of IV, namely utilizing industrial by-product (i.e., sulfur) as main raw material, being atom efficient, and requiring no additional solvents. Hence, some work highlights the utilization of low-cost bulk industrial feedstocks (e.g., dicyclopentadiene), bio-derived renewables (e.g., myrcene, farnesene, and farnesol), repurposed wastes (e.g., used cooking oil) or renewable crosslinkers (e.g., triglycerides, squalene, and perillyl alcohol).

This selection was also motivated to address the susceptibility of the pioneering poly(S-limonene) to re-arrangement and hydrogen loss during synthesis, [34] which can limit the molecular weight (i.e., oligomeric) and glass transition temperature (T_g), consequently reducing the shape-persistence of the IV PS [33–35]. Compared to poly(S-limonene), the synthesized IV PS have indeed higher molecular weights and thus higher T_g values. Furthermore, the rich vinyl and reactive groups of these comonomers were hypothesized to increase sulfur stabilization capacity of the IV PS, which are essentially binding sites for Hg^{2+} adsorption.

However, despite the high sulfur content (i.e., > 40%), most of the IV PS synthesized immediately after poly(S-limonene) (i.e., up to 2018) exhibited low Hg²⁺ adsorption capacities ($q < 26 \text{ mg g}^{-1}$) in aqueous feeds (Table 4). It was observed that the IV PS were hydrophobic due to the rich hydrocarbon and/or aromatic content in the selected comonomers. This hydrophobicity can prevent the IV PS from forming hydrogen bonds with the aqueous feed which concomitantly disfavors Hg²⁺ capture. Furthermore, the high-molecular weight can limit the solubility of the IV

PS in various solvents, thereby making it difficult to process into structures conducive to Hg^{2^+} capture.

At this point, high-molecular weight and shape-persistence of IV PS were taken as new motivations for the development of hydrophilic and processable IV PS effective for Hg²⁺ remediation. Comonomers rich in oxygen-bearing moieties such as –OH, –C=O, and –COOH were employed to synthesize hydrophilic IV PS. Comonomers such as methacrylic acid (MAA) [36,38], 2-carboxyethyl acrylate (CEA) [36,37], and diallyl maleate (DAM) [36] were thus investigated.

In contrast to the typical radical-mediated addition of sulfur diradicals to the vinyl groups of hydrocarbon- and/or aromatic-rich comonomers, spectroscopic and chromatographic analyses (specifically ¹H/¹³C NMR, two-dimensional NMR (HSQC), and GC-MS of the headspace and condensates) suggest that CEA undergoes thermal decomposition into CO2 and acrylic acid, a behavior similar to that observed in polyacrylates and polymethacrylates (Figure 2a) [99–101]. Two main decomposition pathways were proposed (Figure 2b): the first involves molecular ester cleavage, where an acrylic acid group remains attached to the polymer backbone while an acrylic acid molecule is also released, yielding the structure designated as poly(S-CEA)-a. The second route proceeds via homolytic cleavage of the acyl-oxygen bond, resulting in the retention of an ethyl segment in the polymer chain and the release of CO2 and acrylic acid, forming poly(S-CEA)-b. Due to its high abundance among the decomposition products, acrylic acid is also believed to undergo secondary IV with sulfur diradicals, potentially alongside minor contributions from 2-methyl-2-propenoic acid (C₄H₆O₂). This reaction pathway leads to further CO₂ release and the formation of poly(S-CEA)-c. Given the structural similarity between MAA and acrylic acid, it is likely that MAA undergoes analogous reactions with sulfur diradicals,

resulting in poly(S-MAA)-a and poly(S-MAA)-b (Figure 2c), consistent with mechanisms previously reported [99–101]. In contrast, the product from DAM exhibited a clear FTIR spectrum and high polymer yield, supporting the proposed structure poly(S-DAM), although some unreacted vinyl groups may still be present [36] (Figure 2c).

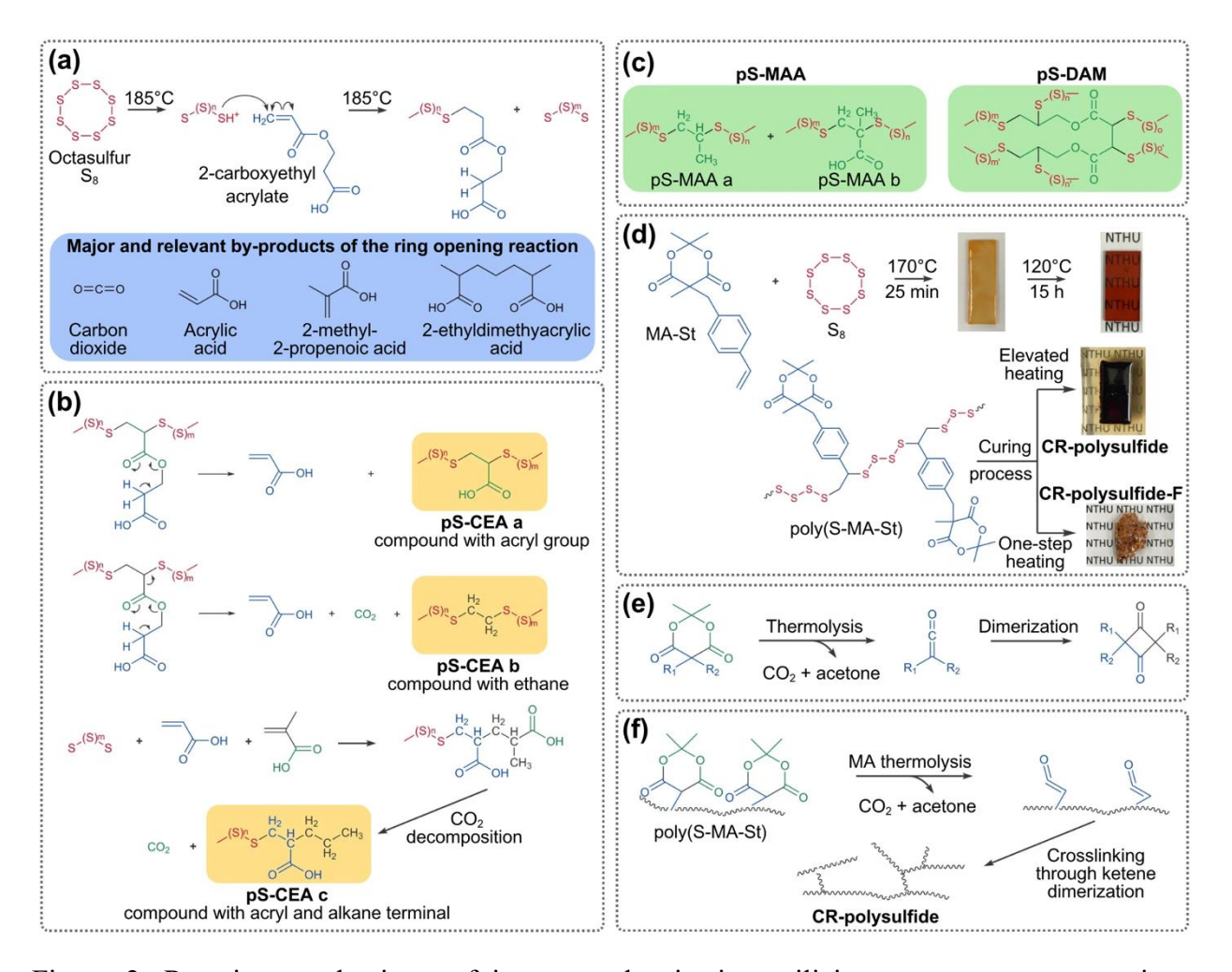


Figure 2. Reaction mechanisms of inverse vulcanization utilizing comonomers to engineer properties of IV PS: (a) ring opening polymerization of S8 with oxygenous 2-carboxyethyl acrylate (CEA) (adapted from Limjuco et al., 2019 [36]); (b) reaction mechanism and structures of poly(S-CEA) (adapted from Limjuco et al., 2019 [36]); (c) structures of other oxygenous IV PS using hydrophilic methacrylic acid (MAA) and diallyl maleate (DAM) (adapted from Limjuco et al., 2019 [36]); (d) reaction mechanism of Meldrum's acid derivative (MA-St) with S8 for preparation of dense cross-linked IV PS (CR IV PS) and foamed CR IV PS (adapted from Lin et al., 2019 [88]); (e) thermolysis reaction of MA group with evolution of CO2 and acetone and the following dimerization reaction of ketene groups (adapted from Lin et al., 2019 [88]); (f)

cross-linking reaction of poly(S-MA-St) through MA thermolysis and ketene dimerization reaction (adapted from Lin et al., 2019 [88]).

The IV PS employing oxygenous comonomers were indeed hydrophilic. However, investigation on the contact angle measurement and O-content shows that the IV PS hydrophilicity is not directly associated with its O-content. Moreover, 1-point adsorption test showed good correlation of adsorption capacity at equilibrium (q_e) and contact angle, indicating strong influence of the IV PS hydrophilicity on Hg²⁺ binding capacity in aqueous feeds (see Section 5). Poly(S-CEA) (at S:CEA molar ratio = 6:1) obtained the highest maximum adsorption capacity ($q_m = 989 \text{ mg g}^{-1}$) [37] so far among the IV PS while amine-impregnated poly(S-MAA) has appreciable q_m (44.7 mg g⁻¹), 20% higher than poly(S-MAA) [38]. It should be noted though that the poly(S-MAA) might have poor distribution with unreacted S-regions indicating incomplete reaction due to MAA volatilization (b.p. 161° C). Hence, the criticality of boiling point in selecting the comonomer for the *conventional* IV.

The IV PS from oxygenous comonomers, particularly CEA, were also oligomeric [poly(S-CEA)] allowing them to be dissolved in common solvents (e.g., non-polar and polar aprotic solvents) which render them processable to different post-processing method (e.g., electrospinning [36] and phase-inversion method [37]. Nonetheless, the IV PS are insoluble in water which is favorable for their minimal elution in water during Hg²⁺ adsorption.

3.2. Characteristics of the IV PS relevant for Hg²⁺ adsorption

Although comonomer selection has served as a fundamental strategy in the design of IV PS for mercury remediation, the underlying rationale has broadened beyond green chemistry principles to encompass the optimization of material properties. These include enhancements in polymer

morphology (i.e., surface area) and engineering of wettability, functionality, reactivity, and topology via multiple component system IV PS.

3.2.1. Morphological enhancement

3.2.1.1. Surface area of pristine IV PS

Surface area is critical in the adsorption performance of IV PS, as it can influence the number of accessible active sites for Hg²⁺ binding. An increased specific surface area enhances the exposure of functional groups, particularly sulfur-rich domains, thereby improving the overall Hg²⁺ uptake capacity [83] through both physisorption and/or chemisorption mechanisms.

Surface area enhancements that have been explored for IV PS for Hg^{2+} binding include foaming using supercritical CO_2 [83], templating using porogens such as NaCl salt [33,35,86,89,91] and polystyrene sulfonate [91], carbonization including KOH-activation [43,85], and *in situ* foaming via CO_2 and acetone evolution [88]. Each strategy offers advantages in enhancing the morphology of the IV PS. Foaming using $scCO_2$ does not only increase the porosity but also increases the T_g of the IV PS by a few degrees. This is attributed to the extraction of trace low molecular weight materials, soluble in $scCO_2$, which would otherwise plasticize the IV PS [83]. Templating using porogens leverages on the cheap and abundant water-soluble porogens [33,35,86,89,91] as well as high control on the IV PS porosity [91].

In carbonization of a particular IV PS system, operation parameters include carbonization temperature and time, with the former showing more significant effect on the IV PS surface area [85]. Poly(S-DCPD) carbonized at 750 °C for 1 and 2 hours yielded $SA_{BET} = 403$ and 415 m² g⁻¹, respectively, whilst that which was carbonized at 850 °C for 1 hour yielded $SA_{BET} = 511$ m² g⁻¹ [85]. Furthermore, carbonization with KOH as activating agent can enhance significantly the

surface area. KOH facilitates porosity development through its reaction with carbon (6KOH + $2C \rightarrow 2K + 3H_2 + 2K_2CO_3$), where in the subsequent thermal decomposition of K_2CO_3 releases CO_2 , contributing to additional pore formation [102]. However, optimum amount of KOH should be determined as oversaturation of KOH can cause micropore collapse [85]. Accordingly, poly(S-DCPD) carbonized at 750 °C for 2 hours at 1:1 KOH:IV PS ratio yielded $SA_{BET} = 2,212$ m² g⁻¹, the highest surface area of IV PS applied to mercury binding application [85]so far.

In relation to the choice of comonomer, another approach in generating porosity to the IV PS *in situ* is selecting a reactive comonomer as in the case of monostyrenic compound containing a Meldrum acid (MA) group [poly(S-MA-styrene)] (Figure 2d) [88]. MA can undergo thermolysis to generate highly reactive ketene groups, featuring CO_2 and acetone molecules, which consequently act as foaming agents to the IV PS (Figure 2e, 2f). Further dimerization generates highly reactive ketene groups which can be effective for further chemical reactions with nucleophiles and self-cycloaddition and dimerization [103–111]. Aside from the Hg^{2+} binding property ($q_e = 51 \text{ mg g}^{-1}$), the synthesized poly(S-MA-styrene) was found to be cross-linkable with repairable features albeit at relatively high temperature and a long thermal treatment time [88]. Thermal treatment induces partial cleavage of the S–S bonds within the cross-linked poly(S-MA-styrene) network, thereby restoring molecular chain mobility. This regained mobility enables the polymer chains to undergo rearrangement and heal damaged regions through chain diffusion and reconnection [88].

Porosity generation via post-IV modification has also been demonstrated via hyper-crosslinking [92]. In this process, poly(S-styrene) was "knitted" using aluminum halide (i.e., AlCl₃) in chloroform at 50 °C to induce crosslinking. This generated a mesoporous IV PS with $SA_{BET} = 236 \text{ m}^2 \text{ g}^{-1}$ and exhibited a Hg²⁺ adsorption of $q_m = 216 \text{ mg g}^{-1}$. Notably, this work highlights that

the adsorption capacity of IV PS is not merely dictated by high surface area or sulfur content alone but rather results from a more nuanced interplay of factors, including hydrophilicity, mesoporosity, and thiol content [92].

3.2.1.2. Composite IV PS configurations

Another approach to improve the morphology of IV PS for Hg²⁺ adsorption involves incorporation into a support material, forming a composite with configurations suited to specific deployment methods (e.g., membrane or column filtration). This also enhances the ease of handling and recyclability of the IV PS for practical applications. Examples of such a strategy include electrospinning [36,84], spin coating and dip coating [87], agar gelation and drop-in-oil method [37], functionalization with magnetic iron oxides [94,112], and scaffolding using mesoporous silica [48,95,113,114].

IV PS can be configured into a fibrous membrane material, as a composite within a polymer matrix, via direct electrospinning [36,84] or dip coating of electrospun fibers [87]. The unique dimensional property of electrospun fibers (i.e., high surface area-to-volume) can shorten Hg^{2+} diffusion distances, enhancing the exposure of IV PS to improve IV PS/feed interaction [36,84]. The ability to select a polymer matrix allows control over the physicochemical properties of the composite IV PS. For example, despite the hydrophobicity of poly(S-DIB), blending it with more hydrophilic poly(methyl methacrylate) (PMMA) to prepare an electrospun poly(S-DIB)/PMMA fiber with a high $q_m = 440 \text{ mg g}^{-1}$ [84]. It was also demonstrated that electrospinning poly(S-CEA) with polyacrylonitrile (PAN) enhanced the utilization of Hg^{2+} binding sites, especially for the S-rich region [36]. This promoted the mechanical and chemical stability of the poly(S-CEA) as demonstrated by recyclability tests and BaSO₄ precipitation tests [including long-term (i.e., 10 months) soaking in 6M HCl stripping solution], where no sign of decomposition to S^{2-} and/or

oxidation to SO₄²⁻ was observed. However, the need to select a polymer matrix can also pose limitations in processing the IV PS via electrospinning as this requires solubility of the IV PS in a common solvent with the polymer matrix. To overcome this, dip coating can be used. For example, electrospun poly(vinyl alcohol) /poly(acrylic acid) (PVA/PAA) was dip coated into poly(S-DIB) dissolved in dichlorobenzene to deposit the IV PS on the surface of the electrospun fibers [87].

Similarly, the agar gelation and drop-in-oil (phase inversion) method enables the configuration of IV PS into microbeads [37], facilitating easy recovery and integration into packed bed columns with favorable hydraulic properties [115]. This approach requires the IV PS to be soluble in a solvent compatible with the hydrophilic agar matrix (e.g., acetone or methanol). Moreover, the morphology of the resulting IV PS beads, including surface area, can be tailored by adjusting formulation parameters such as surfactant addition and pre-blending of the IV PS/agar slurry prior to precipitation in a non-solvent (e.g., hexadecane).

Functionalizing IV PS with magnetic iron oxides can render the composite magnetic IV PS with high specific surface area (1,329 m² g⁻¹) [94] and convenient for retrieval [94,112]. This can be done via precipitation of suspended IV PS (e.g., poly(S-DCPD)) in a mixed solution of FeCl₃ and FeSO₄ [94] or via hot-pressing of IV PS (e.g., poly(S-canola)) with γ -Fe₂O₃ (100°C, 40 MPa, 20 min) [112]. Magnetic poly(S-DCPD) exhibited $q_m = 187.4$ mg g⁻¹ while magnetic poly(S-canola) exhibited at least $q_e = 0.2$ mg g⁻¹ (m = 1.0 g; V = 20 mL; $C_o = 10$ mg L⁻¹; $C_e < 7$ ppb). While this approach is mainly motivated to render the IV PS with good retrievability, this can limit the recyclability of the composite material due to acid dissolution of the magnetic core (i.e., Fe₃O₄ + 8H⁺ \rightarrow Fe²⁺ + 2Fe³⁺ + 4H₂O) which consequently leads to surface leaching and structural

instability, loss of magnetization, and formation of secondary Fe^{2+}/Fe^{3+} precipitates or complexes.

Another strategy in preparing a composite IV PS with tailored characteristics is via scaffolding, using common support materials such as mesoporous silica (e.g., MCM-41), [95] which takes advantage of its controlled size, pore morphology, and facile functionalization [116]. However, it can be expected that the high surface area of MCM-41 ($SA_{BET} \approx 800 \text{ m}^2 \text{ g}^{-1}$) can be significantly reduced by a range of functionalization approaches. For example, from amination [MCM-41-NH₂ ($SA_{BET} \approx 260 \text{ m}^2 \text{ g}^{-1}$)], to functionalization with reactive groups, up to IV to prepare the composite IV PS on mesoporous silica as in the case of sulfur-cross-linked poly(maminothiphenol/potato starch on MCM-41 ($SA_{BET} \approx 20 \text{ m}^2 \text{ g}^{-1}$). Accordingly, the judicious selection of comonomers, with careful consideration of the synthesis route and functionalization of the IV PS, is critical to mitigate the significant reduction of surface area of MCM-41 upon incorporation to the composite IV PS. Poly(S-DCPD) has also been synthesized via direct thermal reaction between sulfur and DCPD at 140 °C. In this case, sulfur reacts across the norbornene double bond to form cyclic polysulfide linkages and subsequent oligomers upon extended heating, rather than through classical ring-opening polymerization of S₈ associated with inverse vulcanization [113]. The resulting poly(S-DCPD) is fully soluble in chloroform, enabling solution-processability and facilitating uniform coating on silica gel (46–63 µm particle size, 60 Å pore size). When evaluated for Hg²⁺ adsorption, the thermally cured poly(S-DCPD)-coated silica exhibited a maximum adsorption capacity of ~5 mg g⁻¹ sorbent (~50 mg g⁻¹ relative to the polymer content). In an equivolume water-diesel system ($C_0 = 5 \text{ mg L}^{-1}$, V = 45 mL; m = 100mg), the material achieved 92% Hg²⁺ removal efficiency [113].

Another noteworthy approach on the preparation of composite IV PS-silica was also exhibited via catalytic inverse vulcanization (see Section 3.3.2). The catalyzed inverse vulcanization of poly(S-limonene) yielded low molecular weight (<1000 $M_{\rm w}$) rendering the IV PS soluble in organic solvents [48]. The metal (i.e., Hg, Au) uptake was observed to be increasing with catalyst (i.e., Zn(DTC)₂) loading which could be due to the contribution of the catalyst itself, which can bind to the metals. The maximum capacity ($q_m = 65 \text{ mg g}^{-1}$) of the composite IV PS-silica corresponds to 716 mg g⁻¹ of IV PS. Detailed kinetic analysis, adsorption-desorption modelling, and adsorption parameters (i.e., pH, ionic strength, and selectivity) evaluation were conducted for this composite Zn-diethyldithiocarcarbamate [Zn(DTC)₂]-catalyzed poly(S-limonene) on silica system [114]. Results showed effective Hg²⁺ adsorption at wide pH range showing no significant Hg²⁺ leaching at pH = 3 to 9 while at pH = 11, the IV PS coating degraded leading to Hg²⁺ release. Kinetic analyses indicate that adsorption at acidic and neutral pH proceed until the available Hg²⁺ and/or accessible sorbent binding sites are exhausted while at basic pH or in the presence of NaCl, binding sites may be limited due to competing reactions [114].

While configuring the IV PS into composite material can help in controlling the physicochemical properties of the IV PS suitable for Hg²⁺ binding, this can also pose challenges to the overall performance of the composite, as observed in a general host adsorbent/support matrix adsorption system [36,37,117,118]. Loading of the IV PS can have a trade-off effect on the stability and adsorption capacity (depending on the IV PS-to-support material amount ratio). The composition of the relatively inert support material and blockage of active sites, especially the rich S-S domains of IV PS, can translate to lower adsorption capacity per unit amount of the composite material. Also, the structure of the bulk material can increase mass transfer resistance of Hg²⁺ from the feed to the IV PS thereby prolonging the time to attain adsorption equilibrium. In the

case of reactive and functional comonomers or support materials, other functional groups can affect the selectivity of the IV PS towards Hg^{2+} . Hence, the careful selection of comonomer and synthesis route in preparing the IV PS, the selection of support material, and the fabrication method to allow high IV PS loading and render it with favorable structural properties, are all critical in designing composite IV PS for Hg^{2+} remediation.

3.2.2. Multi-component system IV PS

Another strategy in improving the properties of the IV PS is the development of a multi-component system to synergize the properties of each component for effective Hg^{2+} adsorption. For example, cottonseed oil (CO)-based IV PS was modified (i.e., cross-linked) with different nitrogen-containing compounds to functionalize the poly(S-CO) with nitrogen-containing functional groups that can also bind with Hg^{2+} [39]. Indeed, it was observed that N-functionalized, especially primary amine, poly(S-CO)s have higher adsorption capacities (80 > q > 125 mg g^{-1}) versus unmodified poly(S-CO) (~69 mg g^{-1}). It was also observed that the addition of the N-containing modifiers increased the surface area (~900 m² g^{-1} versus ~590 m² g^{-1}) although it was not observed to have significant effect on the IV PS adsorption capacity [39].

The same rationale motivated the preparation of hyperbranched polythioamides composed of sulfur, 1,4-diethynylbenzene (DEB), and polyethylene imine (PEI) [40]. This system demonstrated the combined removal ability of N-rich PEI and thioamide with the synthesized poly(S-PEI-DEB) having a very high adsorption capacity (1162 mg g⁻¹). It was observed that a stable chelating structure was formed between Hg²⁺ ions, NH/NH₂, and C=S groups. However, it should be noted that whilst this work has the credentials of IV utilizing elemental sulfur in one-pot and solvent-free reaction system, the PEI becomes the backbone of the poly(S-PEI-DEB), forming C(=S)NH- and -C(=S)N< groups, [40] which deviates from the nature of IV PS where

sulfur is the main backbone of the polysulfide [5]. This is similar to poly(S-MAA-PEI) where sulfur is only 24% *versus* the carbon content which is 54% [38].

Graft copolymerization has also been demonstrated in preparing a ternary IV PS [42]. Cyclooctadiene (Cy) served as a crosslinker while thioacetamide (Tha) served as a grafting monomer. The integration of Tha enhanced sulfur coordination, exposing additional reactive sulfur sites and introducing N-containing moieties, which rendered the poly(S-Tha-Cy) with $q_m = 100 \text{ mg g}^{-1}$.

In other work, ternary systems have been employed to render the polymer with the required hydrophilicity as well as the rich adsorption sites for Hg^{2+} adsorption. For example, hydroxyl groups (-OH) can offer hydrophilicity, Hg^{2+} adsorption sites, and functionalization sites for the IV PS. This was exemplified in a set of work that employed *N*-methyl D-glucamine (NMDG) to impart hydroxyl groups in poly(S-VBC-NMDG; VBC = 4-vinyl benzyl chloride) [41,43]. The NMDG-functionalized IV PS attained high adsorption capacities at $q_m = 572$ mg g⁻¹ [43] and 624 mg g⁻¹ [41].

Similarly, -OH groups from starch render multi-component IV PS effective for Hg^{2+} binding as in the cases of poly(S-starch-oleylamine) [45] and poly(S-starch-cardanol) [44]. Both achieved high adsorption capacities at $q_m = 565$ and 618 mg g⁻¹, respectively. Although similar to the PEI system, while the synthesis involves direct reaction of sulfur with the components, the backbone of the polymer is the starch with a small amount of sulfur (~19 %) [45]. Nevertheless, its function as a Hg^{2+} adsorbent can be effective suggesting the importance of judicious selection of components in designing Hg^{2+} adsorbent, including IV PS.

3.3. Improvement of the inverse vulcanization reaction

Whilst IV is recognized for its green chemistry credentials, the requirement for high synthesis temperatures, typically above the sulfur floor temperature ($T_f = 159$ °C), can limit its practical implementation. Maintaining lower reaction temperatures is essential to reduce the generation of undesirable by-products such as hydrogen sulfide, thiols, etc. and to prevent olefin dehydrogenation [119]. Moreover, operating at reduced temperatures can mitigate the risk of hazardous auto-acceleration associated with the Trommsdorff–Norrish effect, which may arise during the IV reaction [48]. Additionally, numerous potential cross-linkers are unsuitable for use with sulfur in IV due to their insufficient reactivity or low boiling points. In this context, a number of studies focused on reducing the synthesis temperature of IV PS for applications in Hg²⁺ adsorption. These include multicomponent polymerization [40,46], nucleophilic activation [47], catalysis [48], as well as other emerging complementary sulfur-polymer pathways.

3.3.1. Catalyst-free multicomponent polymerization and nucleophilic activation

Multicomponent polymerization (MCP) features high efficiency, simple operation, high atom economy, great structural diversity, and mild conditions, which can provide great opportunity for the direct utilization of sulfur [120–124]. Inspired by catalyst-free MCP of sulfur, alkynes, and aliphatic amines to afford a series of polythioamides at 100 °C [125], an MCP that replaced alkynes with more reactive isocyanides was reported to afford a library of asymmetric thioureas at temperatures from room temperature to 50 °C [126]. This was eventually extended to MCP of elemental sulfur, aliphatic diamines and diisocyanides at room temperature to produce thioureas [46] that were tested for Hg²⁺ adsorption.

In an MCP involving S₈, aliphatic amines, and isocyanides, the reaction is initiated by nucleophilic attack of an aliphatic amine on cyclic S₈, leading to the formation of a zwitterionic ammonium polysulfide intermediate (A) (Figure 3a). The terminal anionic sulfur atom in

intermediate A subsequently attacks the carbenoid carbon of the isocyanide, resulting in the formation of an isothiocyanate intermediate (C). This reactive species then undergoes further nucleophilic addition by a second amine molecule to afford the final thiourea product (D) [126,127].

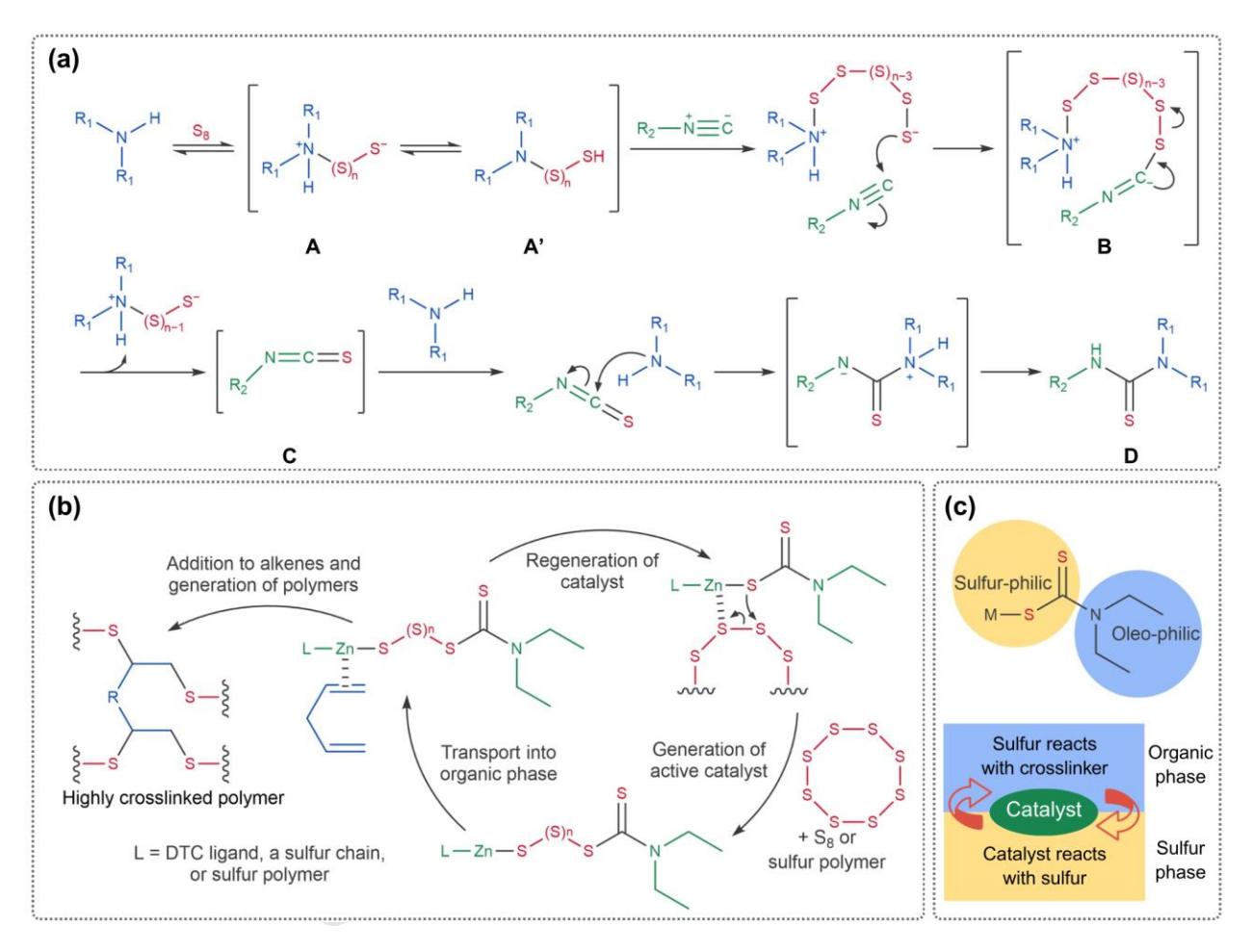


Figure 3. Proposed reaction mechanisms of improved inverse vulcanization: a) multicomponent reaction of sulfur, amine, and isocyanide (adapted from Tian et al., 2018 [46]); b) suggested catalytic cycle for inverse vulcanization (adapted from Wu et al., 2019 [48]); c) representation of the catalyst as a phase transfer agent (adapted from Wu et al., 2019 [48])

The polymerization proceeded rapidly and exhibited broad monomer compatibility, affording 16 polythioureas with well-defined structures, high molecular weights (up to 242,500 g mol⁻¹), and excellent yields (up to 95%). They have high sensitivity to Hg^{2+} ($K_{sv} = 224,900 L mol^{-1}$) and exceptional selectivity. Moreover, they achieve Hg^{2+} removal efficiencies exceeding 99.99%

(i.e., $C_o = 60 \text{ mg L}^{-1}$; $C_e = 1.6 \text{ }\mu\text{g L}^{-1}$; V = 2 mL; m = 2.4 mg; $q_e = 50 \text{ mg g}^{-1}$), meeting drinking water safety standards, while allowing real-time monitoring of the purification process through fluorescence [46]. The same rationale allowed for the preparation of poly(S-1,4-phenylenedimethanamine-PVC) via a substitution reaction of the amine group, nucleophilic activation of sulfur, and S₈ ring-opening reaction at 50 °C for 3 hrs [47]. The poly(S-nucleophile-PVC) achieved a high $q_m = 309 \text{ mg g}^{-1}$, which can be attributed to the affinity of S for Hg²⁺ and the electron-donating ability of N [47]. However, similar to the multi component system, whilst the synthesis involves direct reaction of sulfur with the components, the MCP involves reaction solvent (e.g., DMF/toluene) and the resulting products are polythioureas, with low sulfur ranks compared to IV PS.

3.3.2. Catalytic inverse vulcanization

Catalytic IV has been demonstrated using metal-diethyldithiocarbamate (DTC), which worked with a range of metals including low-cost and non-toxic metals (e.g., Zn, Fe, Co, Cu, Ni, and Na) [48]. Compared to uncatalyzed IV, catalysis reduced the reaction temperature (e.g., 135 °C) and time, improved the stability of the polymers (e.g., increased T_g and improved shape persistency), as also observed in the catalyzed synthesis of poly(S-limonene) (which is otherwise a limitation of the seminal work [32]), and inhibited the production of H₂S gas [48].

In catalytic IV systems, the metal–sulfur (M–S) bond facilitates the opening of the S₈ ring at lower temperatures and enables the insertion of sulfur atoms between the metal center and DTC ligand, thereby generating the active catalyst (Figure 3b). The oleophilic and sulfur-philic groups of the metal-DTC (Figure 3c) enable it to function as an efficient phase-transfer catalyst, facilitating the transport of reactive sulfur into the organic phase. This catalyst effectively positions sulfur in close proximity to the crosslinker, lowering the activation energy required for

bond formation. Whilst the exact mechanistic nature of this step remains uncertain, whether radical, ionic or concerted, it nonetheless promotes efficient sulfur incorporation. Through repeated chain transfer and reaction cycles, the process yields highly crosslinked polymeric networks with a more uniform distribution of sulfur. The conventional RAFT agent, 2-cyano-2-propyl benzodithioate, exhibits no catalytic activity, likely due to its inability to form S–S or M–S bonds, which are essential for sulfur insertion from the S₈ phase and its transport into the organic phase. Whilst the possible catalytic effect could arise from the DTC ligand itself (rather than the metal), it is clear that the more ionic the nature of the M-S bond, the reactivity is higher [48].

Aside from the aforementioned properties improved, the catalyzed IV PS also exhibited improved Hg^{2+} uptake. This was demonstrated by comparing the Hg^{2+} adsorption capacity of catalyzed and uncatalyzed poly(S-limonene)-coated silica gel. The Hg^{2+} uptake increases with catalyst loading [up to $q_m = 65 \text{ mg g}^{-1}$ sorbent catalyzed with 5 wt% Zn-DTC], potentially resulting from improved dispersion and bonding of sulfur, but with a possible contribution from the catalyst itself [48].

3.3.3. Emerging Complementary Sulfur-polymer Pathways

Beyond conventional thermal inverse vulcanization (which often requires high temperatures, may suffer from side-reactions and sulfur loss, and can yield polymers with limited structural control), several new polymerization strategies have emerged that expand the design space for sulfur-rich materials relevant to heavy-metal remediation. Although not all have yet been demonstrated for Hg capture, these approaches provide mechanistic and synthetic advances with clear potential to benefit Hg-sorbent development.

Alternative sulfur-based monomers, i.e., sulfenyl chlorides, expand compositional and architectural control, enabling higher sulfur incorporation and improved network tuning beyond traditional divinyl comonomers, thereby offering pathways to increase sulfur-utilization efficiency [128]. Electrochemical ring-opening polymerization enables low-temperature, electrically controlled polymer growth with reduced side reactions, and improved structural uniformity compared to thermally driven radical processes: features that may translate to improved stability and mass-transfer properties in future adsorption systems [129]. Photo-initiated sulfur ring opening allows ambient-temperature polymer formation with spatial control, lower energy input, and reduced sulfur degradation, which could facilitate the fabrication of high-surface-area or supported architectures advantageous for metal binding [130].

Whilst these methods have been primarily demonstrated for noble-metal capture (e.g., Au, Ag, Cu) or polymer material development, they collectively address key limitations of conventional inverse vulcanization including energy demand, limited structural tunability, and sulfur accessibility. As such, they represent promising and transferable strategies for designing next-generation sulfur-rich materials with enhanced potential for Hg remediation.

4. Hg adsorption performance

Whilst most studies on IV PS focus on material design, characterization, and improvement of the IV reaction, some reports also emphasized critical parameters influencing their application as Hg adsorbent. These include Hg speciation (SI Section 5) and systematic evaluation of mercury adsorption performance, including adsorption thermodynamics evaluation (SI Section 8).

4.1. IV PS cost effectivity vis-à-vis adsorption capacity

In early evaluation studies of IV PS for Hg^{2+} adsorption, initial concentrations of $C_o = 2 - 3$ mg L⁻¹ were commonly used [33,36,83,86]. Adsorption of Hg^{2+} at low concentrations has particular practical relevance [32,83,131]. For example, the Environmental Protection Agency has set a maximum contaminant level goal for mercury of 0.002 mg L⁻¹ or 1 x 10⁻⁶ mg g⁻¹[85]. Hence, the necessity to evaluate the effectivity of IV PS to bind with mercury at low concentration [83,85,92–94]. In this context, some studies emphasized the need for IV PS that demonstrate high Hg^{2+} removal efficiency at low concentrations, rather than material that exhibit high overall capacity but poor uptake performance at trace levels [93]. It has been qualified that, provided the IV PS possesses a reasonable high capacity (e.g., q > 100 mg g⁻¹) and, ideally, a steep uptake profile at low concentrations, it can be effectively utilized for Hg^{2+} removal [94].

It should be noted, however, that maximum adsorption capacity (q_m) , which can be determined through adsorption isotherm experiments, is an important parameter to evaluate the cost effectiveness of the IV PS. Various approaches used for adsorbent cost analysis have adsorption capacity as a cost factor. These include, among others, the cost of adsorbent preparation from the cost of raw materials [132], cost of adsorbent per gram of the adsorbate removed (Eq. 1) [133], and cost of adsorbent preparation using cost indices (Eq. 2) [134].

$$Adsorption \ cost \ \left(\frac{USD}{g_{adsorbate}}\right) = \frac{\left[Chemical \ Purchase \ Cost \left(\frac{USD}{g}\right) + Energy \ Cost \left(\frac{USD*Kw}{g}\right)\right]}{Adsorption \ capacity \left(\frac{mg}{g}\right) x 10^{-3} \left(\frac{g}{mg}\right)}$$
(Eq. 1)

$$Cost \ index = \frac{Adsorption \ capacity\left(\frac{mg}{g}\right)}{Unit \ cost \ of \ adsorbent\left(\frac{USD}{g}\right)}$$
 (Eq. 2)

Economic estimation of poly(S-CEA) indicates that 1 m² of the microfiber could cost around 108 USD [36] if industrial waste sulfur is used as raw material, which only costs 70 USD ton⁻¹. This is equivalent to \sim 0.20 USD per gram of Hg²⁺ (as HgCl₂) recovered based on the physical

properties of the microfiber (i.e., true density and thickness) as well as its maximum adsorption capacity at 30 °C ($q_m = 473 \text{ mg Hg}^{2+} \text{ g}^{-1}$). However, this value only accounts for the raw materials and solvents used for fabrication and does not consider energy consumption for electrospinning, heating for the IV PS synthesis, and labor costs. Nevertheless, with current prices of different industrial membranes (e.g., microfiltration, ultra-filtration, pervaporation, etc.) ranging between 130 - 500 USD m⁻² [135], large-scale production of poly(S-CEA)/PAN microfiber can be feasible for applications in real systems due to cheap cost of sulfur and high Hg²⁺ adsorption capacity of poly(S-CEA)/PAN microfibers. Economic analysis was also conducted to compare carbonized poly(S-VBC)@NMDG to other IV PS (e.g., amine@poly(S-MA) and recently reported unmodified and Na₂S-modified biochar [136] based on (1) cost of producing 1 g of adsorbent and (2) cost of removing 1 g of mercury from wastewater [43]. Carbonized poly(S-VBC)@NMDG was evaluated to be the most cost-effective for mercury removal (9.95 USD g⁻¹ Hg) mainly due to the higher adsorption capacity ($q_m = 572 \text{ mg g}^{-1}$). Whilst the production cost of the amine@poly(S-MA) was only 5.6 USD g⁻¹, its cost per gram of Hg^{2+} removal is significantly higher (126 USD g^{-1} Hg) due to its low adsorption capacity ($q_m =$ 67 mg g⁻¹). These demonstrate the necessity of determining the q_m of the IV PS for mercury adsorption, which can be evaluated through adsorption isotherms at varying initial concentrations.

4.2. Adsorption isotherm evaluation

To realize the common motivation of IV PS as a cost-effective adsorbent for Hg²⁺ removal, it is crucial to establish the most appropriate adsorption equilibrium models. This is indispensable for reliably predicting adsorption parameters and enabling quantitative comparisons of adsorbent performance across different materials and experimental conditions. In this context, adsorption

isotherms, which describe the interaction between pollutants (e.g., Hg^{2+}) and adsorbents (e.g., IV PS), are essential tools for optimizing adsorption mechanisms, elucidating surface properties and capacities, and guiding the rational design of efficient adsorption systems [137]. Different adsorption isotherms, both two-parameter and three-parameter, can be used to model adsorption of environment pollutants (e.g., Hg^{2+} adsorption by IV PS) (SI Section 6 and Table S6).

The accuracy of an isotherm model typically depends on the number of independent parameters, whereas its widespread use often reflects its mathematical simplicity [138]. Linear regression analysis of adsorption isotherm has been frequently employed partly reflecting the simplicity of its equations. However, many studies [137,139–146] observed that the linearized equations generate real problems and errors arising from the complexities and complications for simultaneous transformation of data, leading to the violation of theories behind the isotherms [147].

Linear isotherm analysis assumes normally distributed (i.e., Gaussian) errors with constant variance across all values of the liquid-phase concentration (X-axis) [148]. However, this assumption is rarely valid for adsorption systems, as linearization distorts the inherent nonlinearity of isotherm models and alters error distribution [149]. Studies have shown that linearized forms of the Langmuir and Freundlich models may inaccurately assess model fits and fail to provide meaningful insight into adsorption mechanisms under specific conditions [150]. In contrast, non-linear models retain the original data structure, avoiding such distortions [139]. Whilst some studies have reported comparable results between linear and non-linear methods under certain conditions [150–152], using both approaches can improve the robustness of data interpretation [139]. Regardless of the fitting method, the equilibrium data must be sufficiently comprehensive to ensure accurate and representative isotherm modeling.

4.3. Adsorption kinetics evaluation

Adsorption kinetics govern the uptake rate, which in turn defines the residence time required to complete the adsorption process [118]. Accordingly, various kinetic models (Table S7) can be applied to elucidate the underlying mass transfer mechanisms involved in adsorption (Figure S5). Among these, for Hg²⁺ adsorption using IV PS, the pseudo-first order (PFO) and pseudo-second order (PSO) models are the most common (Table 4 and SI Section 7).

Similarly, due to simplicity [153–158], linearization has been commonly employed to fit the kinetics data and to calculate the parameters q_e and adsorption kinetics rate constants (k_l and k_2) by plotting $\ln(q_e - q_l)$ versus t (for PFO) and t/q_t versus t/q_e (for PSO). However, the linearization of the PFO and PSO model changes the weight of q_t , alters the independent/dependent variables [159], and introduces propagated errors, which leads to the inaccurate calculations of the model parameters [160–162]. In contrast, nonlinear regression techniques can offer more robust and precise parameter estimations [160]. Thus, adopting nonlinear methods for solving adsorption kinetic models is critical for enhancing the reliability of kinetic analyses.

In the study of IV PS for Hg²⁺ binding, PFO and PSO have also been extensively used for the evaluation of the adsorption kinetics [36–40,43–45,47,90,91,94,95,97]. Other adsorption kinetics models used to evaluate the binding of Hg²⁺ to IV PS include Elovich model while the mechanism of the diffusion of Hg²⁺ was also studied by fitting the experimental kinetics data to the linear forms of intraparticle diffusion and liquid film diffusion [91].

4.4. Hg selectivity evaluation

Selectivity is a critical performance metric for IV PS in Hg^{2+} capture applications, as it determines their preferential binding toward Hg^{2+} over coexisting, less hazardous metal ions.

High selectivity not only enhances adsorption efficiency by maximizing Hg^{2+} uptake before saturation but also reduces material consumption and minimizes the generation of secondary waste from non-target metals. These advantages collectively improve the sustainability, operational efficiency, and economic viability of IV PS as sorbents for Hg^{2+} remediation.

Different feedstocks have been used to evaluate the IV PS selectivity. Some studies check the selectivity of IV PS towards Hg²⁺ among other selected cations or heavy metals [42,47,84,98], selection of metal ions in natural water [95], simulated Hg²⁺ solution mixed with other metal ions based on the average acid-extractable metals in agricultural soil [36], simulated chloralkali wastewater [37], actual [37] and simulated [92] river samples, and actual [44,45] and simulated [94,97] industrial wastewaters.

As a soft Lewis acid (SI Section 3), Hg has a good affinity towards sulfur, a soft Lewis base. In fact, reaction thermodynamics show that Hg has higher affinity to sulfur (i.e., $\log K \approx 52.7 - 53.3$) versus Hg to organic matter (i.e., $\log K \approx 22 - 28$) [163]. Hence, the general good selectivity of reported IV PS to Hg^{2+} regardless of the feed profile. Although some reported IV PS with appreciable adsorption capacity towards other semi-/metal ions. Poly(S-styrene) exhibited high affinity towards Sb [92] while poly(S-AVImCl) (AVImCl: 1-allyl-3-vinylimidazolium chloride) has appreciable adsorption capacity to Au^{3+} as well [98].

This selectivity of IV PS to Hg²⁺ has been expressed in different ways. Some works report selectivity by comparing percent (%) adsorbed amount/removal [47,84,92,94,97,98], by evaluating the effect of the coexisting ions on the IV PS Hg adsorption capacity [44,45,95], and by adsorption energy calculation via computational method [42]. However, real feed solutions may not necessarily have equal initial concentration of the coexisting cations which, based on

adsorption isotherm, can have an effect on the adsorption of the adsorbate (i.e., cation). Also, some works do not report other adsorption parameters (e.g., temperature, solid-to-liquid ratio, time), which can also affect the adsorption process. To account for these factors, selectivity parameters such as distribution coefficient (K_D) (Eq. 3), separation factor (α) (Eq. 4), and concentration factor (CF) (Eq. 5) can be employed [36,37,117,118]:

$$K_D = \frac{(C_0 - C_e) \times V}{C_e \times m}$$
 (Eq. 3)

$$\alpha = \frac{K_{D(Hg)}}{K_{D(Me)}}$$
 where $Me =$ competing cations (Eq. 4)

$$CF = \frac{q_{e(Me)}}{C_{0(Me)}}$$
 (Eq. 5)

where C_o is the initial concentration of metal cation (mg L⁻¹), C_e is the concentration of the metal cation at equilibrium (mg L⁻¹), V is the volume of the solution (L), and m is the mass of the IV PS (mg). These parameters can normalize the selectivity of the IV PS towards Hg^{2+} despite the varying initial concentrations of coexisting cations, as in the case of real feed solutions. This can provide conclusive comparison of selectivity parameters among different IV PS for Hg^{2+} adsorption.

5. Maximizing the high S-content of the IV PS for Hg²⁺ adsorption

The well-established rationale for utilizing sulfur in Hg²⁺ remediation – rooted in HSAB theory (SI Section 3), renders sulfur-rich IV PS an ideal Hg²⁺ adsorbent due to its sustainability, cost-effectiveness, and value-adding to industrial by-product in vast surplus, sulfur. To optimize the functionality of sulfur as Hg²⁺-active sites in IV PS, morphology (i.e., surface area and porosity) and wettability have been mainly engineered. Other approach such as functionalization with nitrogen-based moieties has also been explored which can simultaneously improve the IV

reaction (e.g., nucleophilic activation of sulfur with aliphatic amine to allow S_8 ring-opening reaction at 50° C) [47].

The morphology of IV PS - including porosity, surface area, and particle size - can directly affect the diffusion of Hg species and the accessibility of sulfur-rich binding sites. Materials with hierarchical or porous structures provide a greater number of active sites and shorter diffusion paths, thereby enhancing both the rate and capacity of Hg²⁺ uptake [33,83,84]. However, other works observed that specific surface area is not the key factor on the IV PS Hg²⁺ adsorption capacities [39,40].

Diisopropenyl benzene (DIB) has been commonly used as a comonomer for IV PS for Hg^{2+} binding [33,83,84,87] after being employed in the seminal work of IV [5]. However, despite its high S content (i.e., > 40%) [87], poly(S-DIB), even though foamed [83] or coated to nanofibrillar films [87] to increase the surface area, still exhibited low adsorption capacity ($q < 26 \text{ mg g}^{-1}$) [87]. Meanwhile, blending poly(S-DIB) in PMMA fibers achieved high $q_m = 440 \text{ mg}$ g⁻¹ [84]. Whilst the dimensional property of the poly(S-DIB)/PMMA fibers shortens Hg^{2+} diffusion distance and enhances IV PS exposure, the more hydrophilic PMMA matrix could have promoted the contact between the sulfur active sites and Hg^{2+} from the aqueous feed. However, close examination of q and S-loading of poly(S-DIB)/PMMA fibers indicates that it utilized only $\sim 10\%$ of its total S for Hg^{2+} binding [36]. The use of hydrophobic poly(S-DIB) persistently limited the maximum utilization of the S-based active sites. This exhibits that whilst morphology engineering can enhance the adsorption capacity of the IV PS for Hg^{2+} binding at aqueous system, wettability of the IV PS governs the interfacial contact between the sulfur active sites and the Hg species.

In this context, to fully maximize the ideality of sulfur-rich IV PS as adsorbents for Hg^{2+} adsorption, it is critical to evaluate the sulfur utilization efficiency (i.e., % sulfur or binding site utilization) based on the adsorption capacity of the IV PS and the assumed S:Hg complexation (e.g., 2:1) [164]. This active site utilization efficiency can also be extended to other functional groups (e.g., O- or N-moieties) once their participation in Hg^{2+} binding has been established. This requires intensive characterization: (1) quantification of elemental composition (e.g., elemental analysis); (2) elucidation of the structure of the IV PS and therefore, the type of functional groups present [e.g., FTIR, NMR (^{1}H , ^{13}C , HSQC), XPS analyses]; (3) determination of participation of functional groups to Hg^{2+} binding [e.g., FTIR, XPS analyses]; (4) evaluation of IV PS Hg^{2+} adsorption capacity (e.g., 1-point adsorption at particular C_0 or adsorption isotherm); (5) quantification of % binding site utilization per unit amount of IV PS, as in the case of sulfur as active binding sites (Eq. 6) [36]:

% binding site utilization =
$$\frac{q_e \, or \, q_{max} \left(\frac{mg \, Hg^{2+}}{g \, IV \, PS}\right)}{S \, content \, (moles)*Hg:S \, binding \, ratio \left(\frac{mole \, Hg}{mole \, S}\right)*Hg \, MW} \, x \, 100\%$$
(Eq. 6)

In the case of IV PS prepared from oxygenous comonomers (i.e., MAA, CEA, and DAM), contact angle measurement indicated that IV PS hydrophilicity is not directly associated with Ocontent, but with the type and number of present oxygenous groups (e.g., hydroxyl, carbonyl) and that hydrophilicity can have strong influence on Hg²⁺ binding capacity [36,37]. To validate this hypothesis, hydration number [165] of the IV PS was evaluated.

Hydration number (n_H = number of H₂O molecules per functional group) is one of the most quantitative parameters that measures the extent of hydrophilicity of a compound [165]. Previous

studies have classified carbonyl C=O as "hydroneutral" with $n_H = 0$ whereas -OH is a hydrophilic moiety with $n_H = 5$ (Table 5).

Table 5. Values of $n_{\rm H}$ for typical polar groups at 25°C.

Polar	Nitro	Cyano	Carbonyl	Ester	Ether	Hydroxy	Amide
groups							
Structure	$-NO_2$	-CN	-C(=O)-	_	_	–OH	_
				C(=O)O-	CH ₂ OCH ₂ -		$C(=O)NH_2$
$n_{ m H}$	0	0	0 [166]	0 [166]	4 [167,168]	5 [169]	6 [170]
	[165]	[165]					

For the IV PS prepared from oxygenous comonomers, the total hydration number (*HN*) was estimated via material balance given the O-content of pure IV PS (Eq. 7):

Total hydration number (H₂O molecules g⁻¹) HN x 10²²

$$= \frac{o \text{ (wt\%)}}{100} \times \frac{mole}{g \text{ (MW O)}} \times \frac{1 \text{ mole O (-OH)}}{2 \text{ moles O (-COOH)}} \times N_A \times n_H$$
 (Eq. 7)

Where:

- MW of oxygen = $15.999 \text{ g mole}^{-1}$
- The divisor 2 is to account for only half the O content for -OH groups as total O-content (wt%) accounts for the entire -COOH groups
- $N_A = Avogadro's number = 6.022 \times 10^{23} OH groups mole^{-1}$
- $n_H = 5 \text{ H}_2\text{O}$ molecules per -OH group (Table 5)
- $n_H = 0$ H₂O molecules per C=O group, hence poly(S-DAM) has 0 total hydration number.

A strong inverse correlation between the contact angle and HN was observed, which further suggests that IV PS hydrophilicity is indeed not directly correlated to its O-content but rather, to the type and number of present oxygenous groups (Figure 4a). Direct correlation was also observed between S-content and q_e (assuming 2 S:1 Hg²⁺ complexation) (Figure 4b). Likewise,

direct correlation was observed between % binding site utilization and HN (Figure 4c). Under the same C_o , poly(S-DAM), poly(S-MAA), and all poly(S-CEA) are colinear wherein the more hydrophilic IV PS is, the higher the extent of its binding sites are utilized for Hg^{2+} (Figure 4c). This suggests that S-content increases q_e whereas HN of IV PS enhances % binding site utilization. However, these observations remain true if and only if, the IV PS is well-hydrated as S:CEA optimization shows that at S:CEA molar ratio = 8:1, the poly(S-CEA) are nearly hydrophobic (CA = 82°) and already deviated from the said observations (Figure 4d) [37]. Simply, as long as the feed has intimate contact with the IV PS, the number of its available Hg^{2+} binding sites becomes the determining parameter for its q_e value although HN governs the binding site utilization. This points out the importance of IV PS hydrophilicity on the accessibility of the binding sites for Hg^{2+} adsorption.

Performance of IV PS from the literature evaluated from similar $C_o = 2 - 3$ mg L⁻¹ were extracted with the needed physicochemical properties data (e.g., contact angle, elemental analysis, and q_e) and were plotted (Figure 4e). Other IV PS from literature have significantly high S-content (> 40 wt%) which questions their low q_e values. Inspection of their chemical structures reveals that all IV PS have no hydrophilic or polar moieties except for S-farnesol, which has a single -OH group. Thus, if their q_e values are plotted against their total $HN \sim 0$, these materials can be found at the lower left corner of the plot (Figure 4e) while IV PS which remains well-hydrated with satisfactory physicochemical properties is expected to achieve the highest q_e (upper right of Figure 4e), as in the case of poly(S-CEA) at S:CEA molar ratio = 6:1 with $q_m = 989$ mg g⁻¹ [37].

Configuring the IV PS to an electrospun microfiber in composite with polyacrylonitrile (PAN) further enhanced the binding site utilization. Poly(S-CEA) at S:CEA molar ratio = 2:1 exhibited

33% binding site utilization (i.e., S-rich region) which was enhanced up to 53 - 68% upon electrospinning it with PAN at 150 wt% [36]. This highlights the benefit of increasing the surface area (e.g., electrospinning) in improving the accessibility of the Hg^{2+} binding sites. This also clearly points out the important synergy of high S-content, hydrophilicity, and surface area of IV PS to achieve high q and maximize the % binding site utilization of the sulfur-rich IV PS.

In this context, it is essential to elucidate how the support material influences the adsorption mechanism and overall performance of IV-PS systems (Section 3.2.1.2). In addition to increasing surface accessibility in solid IV PS matrices and employing high-surface-area supports to expose sulfur sites, an emerging approach is the use of water-soluble or dispersible IV PS-derived polysulfides that present sulfur directly in solution. In these systems, metal capture proceeds via coordination-driven flocculation rather than surface adsorption, enabling near-maximal sulfur exposure and efficient metal-sulfur binding. Representative examples include water-soluble poly(S-AVImCl) for Hg²⁺ removal [98], poly(S-diallyldimethylammonium chloride) for Au³⁺ and Ag⁺ adsorption [171], and poly(S-norbornene derivatives), synthesized via electrochemical polymerization, for Cu²⁺ recovery [129]. In any case, to fully assess and optimize these approaches, rigorous material characterization and mass-balance analyses are necessary to quantify binding site utilization and sulfur participation, thereby enabling rational design strategies that maximize sulfur deployment in the IV PS network and enhance adsorption performance.

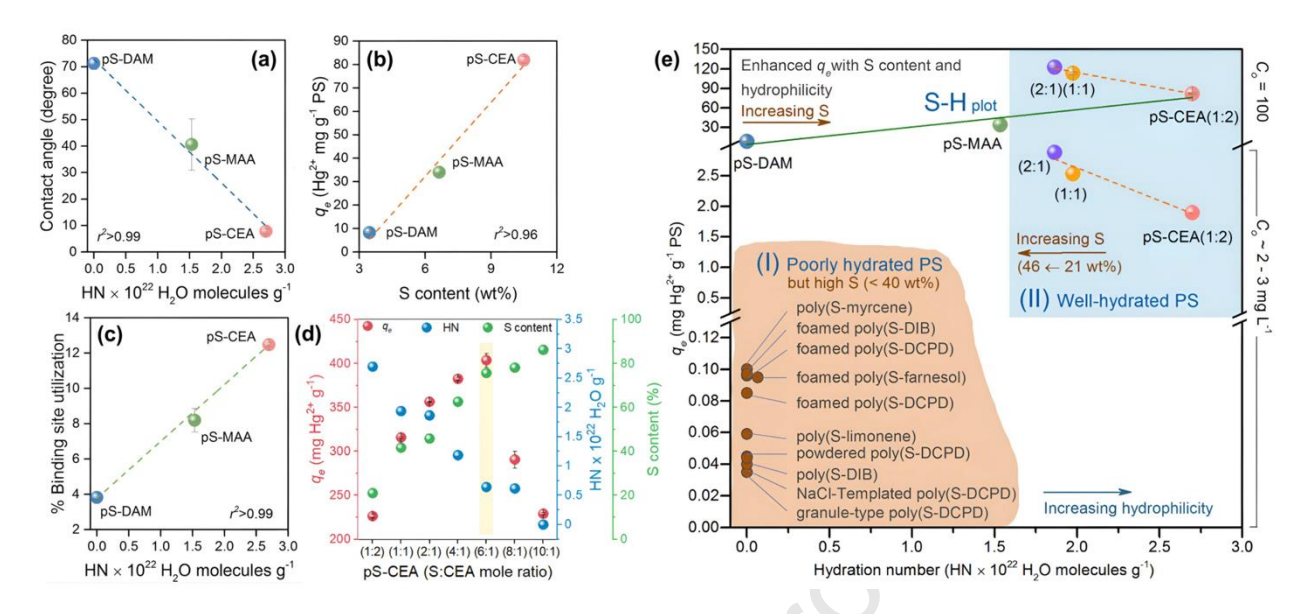


Figure 4. Performance evaluation of hydrophilic IV PS synthesized using oxygenous comonomers (adapted from Limjuco et al., 2019 [36]): a) contact angle vs. hydration number (HN) plot; b) adsorption capacity vs. S content plot; c) % binding site utilization vs. HN plot; d) optimization of poly(S-CEA) with respect to adsorption capacity, HN, and S content (adapted from Limjuco et al., 2020 [37]); e) adsorption capacity vs. HN plot of some IV PS.

6. Theoretical and computational studies on IV PS for Hg²⁺ adsorption

In the advent of digital technology, machine learning (ML), an advanced tool rooted in computer science and artificial intelligence, enables the modeling of complex, nonlinear relationships by learning from empirical data to build highly accurate predictive regression models [172]. By forecasting experimental outcomes, guiding design optimization, and minimizing redundant trials, ML enhances both experimental efficiency and resource utilization [173]. Crucially, ML models can generalize to unseen data, improving performance in real-world applications. In environmental science, ML has recently gained traction for predicting phenomena such as urban CO₂ emissions [174] and CO₂ capture capacity of MOFs [175], radionuclide migration in groundwater [176], and biochar's [177] and bentonite's [172] heavy metal adsorption capacity. In heavy metal adsorption studies, adsorbent's adsorption capacity is influenced by multiple interrelated factors – adsorbent properties, adsorption conditions, and the nature of target metals.

Traditional experimental approaches are often time-consuming, resource-intensive, and limited in generalizability. ML, by contrast, excels in handling such high-dimensional data [178], offering a powerful means to develop accurate predictive models and accelerate the practical deployment of adsorbents for heavy metal remediation.

In IV PS system, ML has been employed to predict the Hg²⁺ removal efficiency (% Hg²⁺ removal) of NMDG-functionalized poly(S-VBC) inverse vulcanized polymers (IV PS), using algorithms such as Gaussian Process Regression (GPR), Artificial Neural Networks (ANN), Decision Trees, and Support Vector Machines (SVM) [41]. Comprehensive hyperparameter tuning and loss function optimization were performed to minimize prediction errors. Among the models, the optimized GPR algorithm exhibited superior predictive accuracy, achieving high coefficients of determination ($R^2 = 0.99$ for training and 0.98 for unseen data) and low root mean square errors (RMSE = 2.74 for training and 2.53 for unseen data). The models were trained on experimental datasets where initial Hg²⁺ concentration, adsorption time, and solution pH were systematically varied. To validate the GPR model, an experimental study was conducted under selected conditions (pH = 6, adsorption time = 4 h, C_o = 60 mg L⁻¹), yielding a near-perfect agreement between predicted and actual values (99.95% accuracy). These results underscore the robustness and reliability of the GPR approach for modeling Hg^{2^+} adsorption behavior under defined conditions. However, further model refinement incorporating additional influential variables, such as adsorbent dosage (solid/liquid ratio), temperature, and multicomponent system effects, is necessary to enhance generalizability across broader environmental scenarios.

Computational fluid dynamics (CFD) modeling offers a comprehensive analytical approach to bridge lab-scale experiments with pilot and industrial-scale applications. It serves as a mathematical framework for examining complex systems involving interactions between fluids

and gases, fluids and solids, or multiple fluid phases, utilizing differential equations to capture the physical behavior of fluid dynamics. CFD enables accurate prediction of how fluid flow conditions (e.g., temperature, concentration, velocity, and viscosity) affect processes like adsorption, using simulation tools like ANSYS or COMSOL Multiphysics.

In the case of IV PS for Hg^{2^+} adsorption, CFD analysis was also employed to analyze the adsorption capacities of porous poly(S-DVB)s foamed using NaCl and poly(sodium 4-styrene sulfonate) (PSS) [82]. Initial and boundary conditions for the porous-zone CFD model include C_o (2 – 6 mg L⁻¹), IV PS thickness (2 – 5.5 cm), initial volumetric feed flow rate (2.86 – 4.62 μ m³ s⁻¹), and initial temperature (300 – 380 K) at constant outlet pressure (0 atm). Eulerian multiphase model was applied using CFD ANSYS Fluent where Eulerian dual fluid model allows the simulation of several distinct phases that interact with each other versus Eulerian-Lagrangian approach which employs discrete phase model [82]. The CFD model results were validated with experimental results at fixed and varied operational conditions which showed consistent results. PSS-foamed IV PS (porosity = 59.09%; ρ = 0.53 g cm⁻³; particle size = 20 – 50 μ m) exhibited experimental q = 244 μ g g⁻¹ versus CFD simulation q = 249 μ g g⁻¹. This CFD analysis can help optimize the process conditions and predict suitable operational parameters for scaling-up the Hg^{2^+} remediation using IV PS.

7. Practical deployment considerations: safety, scalability, regeneration, and sustainability

Outlining the diverse motivations driving their development, IV PS for mercury remediation clearly exemplify the structure–property–performance–processing (SP³) paradigm, underscoring how molecular design, network architecture, and fabrication approaches collectively determine functionality and scalability. This SP³ framework not only explains material behavior but also informs pathways toward advancing the technology readiness level of IV PS to large-scale

deployment. Beyond intrinsic adsorption performance, the practical implementation of IV PS for Hg remediation requires careful consideration of manufacturability, operational safety, regeneration, and life-cycle sustainability: factors systematically aligned with the SP³ paradigm (Table 6).

Although IV PS are typically produced without additional solvent melt polymerization and benefit from low-cost, abundant sulfur feedstocks, molten-sulfur processing introduces thermal and gas-emission hazards. Safe scale-up therefore necessitates precise temperature control, appropriate reactor engineering, and effective off-gas management (e.g., H₂S monitoring and scrubbing). Emerging low-temperature, catalytic, and mechanochemically assisted inverse vulcanization strategies aim to reduce these risks and energy requirements. However, these innovations can introduce trade-offs. For instance, photo-induced inverse vulcanization enables ambient-temperature synthesis with reduced sulfur degradation and spatially controlled curing, yet may require extended irradiation times (e.g., ~72 h) [78]. Nevertheless, such approaches are compatible with next-generation fabrication platforms, including additive manufacturing (e.g., 3D printing), to tailor sorbent morphology and maximize interfacial surface area for applicationspecific Hg remediation. The low cost of sulfur as the primary feedstock also supports the economic feasibility of electrospinning as a fabrication route, enabling the production of IV-PSbased materials with tunable physicochemical properties [36]. Likewise, templating with inexpensive sacrificial porogens such as NaCl offers a cost-effective strategy to generate porous IV-PS sorbents [33,35,86,89,91]. More broadly, scalability prospects remain promising through continuous melt-processing tools and catalytic polymerization routes that enhance process efficiency.

Table 6. Key practical considerations for IV PS in mercury remediation.

Dimension	Key Challenges	Opportunities & Strategies	Metrics / Evaluation Tools
Safety in Manufacture	High-temp sulfur melt; risk of H ₂ S release; volatile monomers	Closed systems, ventilation, scrubbing, catalytic/low-T	Safe temp range, H ₂ S monitoring, risk controls
Scalability	Heat/mixing uniformity; batch variability	processes Extrusion, scalable catalysts, renewable monomers	Throughput, energy kWh/kg, reproducibility
Regeneration & Reuse	Strong Hg–S binding, potential polymer fatigue	Mild eluents, swelling-aided regeneration, composite supports	Regen cycles to ≥80% capacity, leach tests
End-of-Life	Hg release risk; hazardous waste management	Encapsulation, vitrification, immobilization	Toxicity Characteristic Leaching Procedure (TCLP), Hg mass balance
Environmental Sustainability (LCA)	Quantifying 'green' advantage; processing energy	By-product sulfur, renewable comonomers, LCA-guided design	GHG footprint, energy intensity, circularity
Economic Viability (TEA)	Competition with activated carbon/ion-exchange	Low-cost feedstocks, modular production, reuse	Cost per m³ treated; CAPEX/OPEX

Regeneration and reuse are central to techno-economic viability. While IV PS often demonstrate strong and, in some cases, irreversible Hg–S binding, several studies report successful regeneration using mild eluents or swelling-assisted desorption (Table 4). Nonetheless, systematic evaluation of polymer integrity, retention of active sulfur sites, and safe handling of eluates remains essential. End-of-life management is equally critical; mercury-laden IV PS may require immobilization strategies such as encapsulation or vitrification to eliminate release risk, reinforcing the importance of designing systems suitable for circular handling and secure disposal.

Life-cycle assessment (LCA) has emerged as a key tool for verifying the environmental advantages of sulfur-based sorbents. Recent LCAs on sulfur polymer platforms represent

pioneering progress and highlight the need to quantify energy inputs, feedstock sourcing, and end-of-life pathways to substantiate green-chemistry claims [78,179]. Moving forward, integrating LCA with techno-economic analysis and circular-design principles will be essential for optimizing material formulation, identifying sustainability trade-offs, and ensuring IV PS-based sorbents achieve both high performance and demonstrable environmental responsibility in mercury-remediation applications.

8. Summary and Outlook

Since its first report in 2013, inverse vulcanization has garnered increasing attention. This interest is driven by its versatility in producing sulfur-rich polysulfides with diverse applications, adding significant value to an abundant, readily available, and cheap raw material – sulfur. Its simplicity, low cost, non-addition of additional solvent, and high atom economy highlight its potential for scalable sulfur valorization. Among the diverse applications, a particularly compelling and chemically rationalized use is in the adsorption of heavy metals, especially mercury – a detrimental priority pollutant. This compounds the green chemistry credentials of the IV PS rendering it an ideal, cost-effective Hg²⁺ adsorbent.

Different IV PS have been designed and evaluated for Hg remediation since its first proof using poly(S-limonene) showing selective chromogenic response to Hg²⁺ [32]. This development is motivated by the choice of comonomer; characteristics of the IV PS which include enhancement of morphology and engineering of wettability, functionality, reactivity, and topology via multiple component system; improvement of the IV reaction (e.g., catalyst-free multicomponent polymerization and nucleophilic activation and catalysis; evaluation of different factors affecting the performance of IV PS as Hg²⁺ adsorbent and more recently; theoretical and computational studies (e.g., machine learning, density functional theory, and computational fluid dynamics

studies). These motivations have indeed rendered IV PS as an emerging Hg^{2+} adsorbent in terms of structure (i.e., enriched Hg^{2+} adsorption sites), processing (i.e., improved atom-efficient IV reaction at $T < T_f$ at ~159°C) and properties (esp. processability, morphology, and wettability).

Nevertheless, performance-wise, there remain a number of areas in which research on IV PS for Hg adsorption can be enhanced. Key aspects include: (1) normalization of performance parameters evaluation (i.e., adsorption isotherm, kinetics, and selectivity); (2) normalization of adsorption capacity reporting (i.e., q_e vs. q_m) vis-à-vis evaluation and establishment of cost-effectiveness of the IV PS; (3) maximizing the high S-content of the IV PS for Hg²⁺ adsorption; (4) leveraging on the emerging digital technologies; and (5) evaluation of sustainability and techno-economic aspect of the IV PS for Hg remediation.

Comparing performance across studies remains challenging due to variations in testing conditions, analytical methods, and reporting metrics. Establishing standardized evaluation protocols, at least in specifying key parameters, would enable reproducibility, facilitate cross-study benchmarking, and accelerate material optimization. Key parameters include (1) sorbent dosage or solid-to-liquid ratio; (2) initial mercury concentration; (3) contact time (and agitation speed); (4) solution chemistry (e.g., pH and ionic strength); (5) temperature; and (6) mercury speciation.

Whilst linear regression analyses of adsorption isotherm and kinetics have been employed partly reflecting the simplicity of its equations, it can generate errors arising from the complexities and complications for simultaneous transformation of data, leading to the violation of theories behind the models. Hence, comparative studies between linear and non-linear, complemented by quality-of-fit evaluation (R², RMSE), can improve the robustness of data interpretation. Selectivity evaluation of IV PS to Hg²⁺ should also be standardized and should have sound

rationale on the feed composition profile vis-a-vis its practical relevance. It is highly recommended to employ selectivity parameters such as distribution coefficient (K_D) (Eq. 3), separation factor (α) (Eq. 4), and concentration factor (CF) (Eq. 5) to normalize varying adsorption parameters.

Some works have qualified that for as long as IV PS possesses a reasonable high capacity (e.g., > 100 mg g^{-1}) and a steep uptake profile at low concentrations; IV PS can be effectively utilized for Hg²⁺ removal. This justifies the employment of low concentration Hg²⁺ feed (e.g., $2-3 \text{ mg L}^{-1}$). Whilst this indeed has particular relevance, it should be noted though that the maximum adsorption capacity (q_m), which can be determined through adsorption isotherm experiments at different C_o , is an important parameter to evaluate the cost-effectiveness of the IV PS. Building on this, it is also important to include techno-economic studies on IV PS as Hg²⁺ adsorbent to truly establish its cost-effectiveness.

The rich sulfur-based functional groups of the IV PS render it to be theoretically high-capacity Hg^{2+} adsorbent. However, just like the other adsorbents for heavy metal sorption [180], IV PS lack in quantitative assessment of functional group's role in Hg^{2+} sorption. In this context, to fully maximize the functionality and reactivity of IV PS as Hg^{2+} adsorbents, it is critical to evaluate its functional group, particularly the sulfur-based, utilization efficiency (i.e., % binding site utilization). This requires intensive characterization: (1) quantification of elemental composition (e.g., elemental analysis); (2) elucidation of the structure of the IV PS and therefore, the type of functional groups present [e.g., FTIR, NMR (^{1}H , ^{13}C , HSQC), XPS analyses]; (3) determination of participation of functional groups to Hg^{2+} binding [e.g., FTIR, XPS analyses]; (4) evaluation of IV PS Hg^{2+} adsorption capacity (e.g., 1-point adsorption at particular C_o or adsorption isotherm); (5) quantification via material balance of % binding site utilization per unit

amount of IV PS. This can effectively provide mechanistic and empirical insights in designing IV PS, for example, by engineering its morphology or focusing on improving its wettability visà-vis loading of hydrophobic sulfur-based functional groups.

Future opportunities in sulfur-polymer sorbent development lie in expanding beyond conventional thermal inverse vulcanization toward milder, more controlled polymerization strategies. Recent advances including alternative sulfur-based monomers, electrochemical sulfur ring-opening polymerization, and photo-initiated sulfur polymerization, demonstrate that high-sulfur materials can now be synthesized with improved structural control and reduced energy input. Although these methods have so far been applied mainly to noble-metal binding and other functional materials, they present promising routes to tune sulfur accessibility, network architecture, and processability for mercury-remediation systems. Looking forward, adapting these controlled polymerization strategies to Hg-binding frameworks, while simultaneously integrating design principles for wettability, selectivity, recyclability, and sulfur-utilization efficiency, may accelerate the development of next-generation, scalable, and environmentally sustainable sorbents for mercury removal.

To fully realize the practical advantage of IV PS for Hg remediation, digital technologies can be employed to translate its lab-scale results. ML can enhance both experimental efficiency and resource utilization by forecasting experimental outcomes, guiding design optimization, and minimizing redundant trials. Meanwhile, CFD modeling enables accurate prediction of how fluid flow conditions (e.g., temperature, Hg²⁺ concentration, velocity, and viscosity) and IV PS system boundary conditions (e.g., thickness, particle size) can affect Hg²⁺ adsorption on IV PS systems.

Lastly, to close the loop on the green chemistry credentials of IV PS as Hg²⁺ adsorbents, its sustainability should be established, which otherwise, can still be lacking in the current literature.

For example, Life Cycle Assessment (LCA) is essential for evaluating the true sustainability of IV PS as Hg²⁺ adsorbents. Whilst IV PS are often lauded for their green credentials, owing to the use of industrial byproduct sulfur and, in some cases, renewable comonomers, these claims must be substantiated through quantitative environmental impact analysis. LCA enables a cradle-to-grave assessment of IV PS synthesis, application, and disposal, allowing for comparison against conventional Hg adsorbents such as activated carbon or thiol-functionalized materials. Moreover, LCA highlights trade-offs between material performance and hidden environmental burdens, such as energy-intensive polymerization, solvent use, or the environmental fate of mercury-laden polymers. This becomes particularly critical when considering end-of-life scenarios, where improper disposal could risk secondary contamination. As mercury remediation technologies increasingly fall under regulatory and funding scrutiny, especially in the context of the Minamata Convention, incorporating LCA into IV PS development ensures that material innovation aligns with environmental responsibility and policy compliance.

Acknowledgement

L.A.Limjuco would like to acknowledge the support of the Early Career Fellowships Scheme under the International Science Partnerships Fund (ISPF), managed by the UK Department for Science, Innovation and Technology (DSIT) and delivered by the British Council.

References

- [1] Mineral Commodity Summaries: Sulfur, United States Geological Survey, 2024. https://pubs.usgs.gov/publication/mcs2024.
- [2] J.-G. Wagenfeld, K. Al-Ali, S. Almheiri, A.F. Slavens, N. Calvet, Sustainable applications utilizing sulfur, a by-product from oil and gas industry: A state-of-the-art review, Waste Manag. 95 (2019) 78–89. https://doi.org/10.1016/j.wasman.2019.06.002

- [3] M. Maslin, L. Van Heerde, S. Day, Sulfur: A potential resource crisis that could stifle green technology and threaten food security as the world decarbonises, Geogr. J. 188 (2022) 498–505. https://doi.org/10.1111/geoj.12475.
- [4] S. Penczek, R. Ślazak, A. Duda, Anionic copolymerisation of elemental sulphur, Nature 273 (1978) 738–739. https://doi.org/10.1038/273738a0.
- [5] W.J. Chung, J.J. Griebel, E.T. Kim, H. Yoon, A.G. Simmonds, H.J. Ji, P.T. Dirlam, R.S. Glass, J.J. Wie, N.A. Nguyen, B.W. Guralnick, J. Park, Á. Somogyi, P. Theato, M.E. Mackay, Y.E. Sung, K. Char, J. Pyun, The use of elemental sulfur as an alternative feedstock for polymeric materials, Nat. Chem. 5 (2013) 518–524. https://doi.org/10.1038/nchem.1624.
- [6] A. Duda, S. Penczek, Anionic copolymerisation of elemental sulfur with 2,2-dimethylthiirane, Makromol. Chem. 181 (1980) 995–1001. https://doi.org/10.1002/macp.1980.021810503.
- [7] L.B. Blight, B.R. Currell, B.J. Nash, R.T.M. Scott, C. Stillo, Chemistry of the modification of sulphur by the use of dicyclopentadiene and of styrene, Br. Polym. J. 12 (1980) 5–11. https://doi.org/10.1002/pi.4980120103.
- [8] T. Tsuda, A. Takeda, Palladium-catalysed cycloaddition copolymerisation of diynes with elemental sulfur to poly(thiophene)s, Chem. Commun. (1996) 1317. https://doi.org/10.1039/cc9960001317.
- [9] Y. Ding, A.S. Hay, Copolymerization of elemental sulfur with cyclic(arylene disulfide) oligomers, J. Polym. Sci., Part A: Polym. Chem. 35 (1997) 2961–2968. https://doi.org/10.1002/(SICI)1099-0518(199710)35:14%3C2961::AID-POLA17%3E3.0.CO;2-H.
- [10] W.J. Chung, A.G. Simmonds, J.J. Griebel, E.T. Kim, H.S. Suh, I.B. Shim, R.S. Glass, D.A. Loy, P. Theato, Y.E. Sung, K. Char, J. Pyun, Elemental sulfur as a reactive medium for gold nanoparticles and nanocomposite materials, Angew. Chem. Int. Ed. 50 (2011) 11409–11412. https://doi.org/10.1002/anie.201104237.
- [11] Z. Huang, Y. Deng, D.H. Qu, Adding value into elementary sulfur for sustainable materials, Chem. Eur. J. (2025) e202500125. https://doi.org/10.1002/chem.202500125.
- [12] A.K. Mann, L.S. Lisboa, S.J. Tonkin, J.R. Gascooke, J.M. Chalker, C.T. Gibson, Modification of polysulfide surfaces with low-power lasers, Angew. Chem. Int. Ed. 63 (2024) e202404802. https://doi.org/10.1002/anie.202404802.
- [13] K. Wei, K. Zhao, Y. Gao, H. Zhang, X. Yu, M.-H. Li, J. Hu, Near-infrared-light responsive degradable polysulfide pesticide carriers by one-pot inverse vulcanization, Chem. Eng. J. 462 (2023) 142191. https://doi.org/10.1016/j.cej.2023.142191.

- [14] S.J. Tonkin, L.N. Pham, J.R. Gascooke, M.R. Johnston, M.L. Coote, C.T. Gibson, J.M. Chalker, Thermal imaging and clandestine surveillance using low-cost polymers with long-wave infrared transparency, Adv. Opt. Mater. 11 (2023) 2300058. https://doi.org/10.1002/adom.202300058.
- [15] J. Pyun, R.A. Norwood, Infrared plastic optics and photonic devices using chalcogenide hybrid inorganic/organic polymers via inverse vulcanization of elemental sulfur, Prog. Polym. Sci. 156 (2024) 101865. https://doi.org/10.1016/j.progpolymsci.2024.101865.
- [16] J.J. Griebel, S. Namnabat, E.T. Kim, R. Himmelhuber, D.H. Moronta, W.J. Chung, A.G. Simmonds, K. Kim, J. van der Laan, N.A. Nguyen, E.L. Dereniak, M.E. Mackay, K. Char, R.S. Glass, R.A. Norwood, J. Pyun, New infrared transmitting material via inverse vulcanization of elemental sulfur to prepare high refractive index polymers, Adv. Mater. 26 (2014) 3014–3018. https://doi.org/10.1002/adma.201305607.
- [17] F. Wu, S. Chen, V. Srot, Y. Huang, S.K. Sinha, P.A. van Aken, J. Maier, Y. Yu, A sulfur–limonene-based electrode for lithium–sulfur batteries: high-performance by self-protection, Adv. Mater. 30 (2018) 1706643. https://doi.org/10.1002/adma.201706643.
- [18] A.G. Simmonds, J.J. Griebel, J. Park, K.R. Kim, W.J. Chung, V.P. Oleshko, J. Kim, E.T. Kim, R.S. Glass, C.L. Soles, Y.-E. Sung, K. Char, J. Pyun, Inverse vulcanization of elemental sulfur to prepare polymeric electrode materials for Li–S batteries, ACS Macro Lett. 3 (2014) 229–232. https://doi.org/10.1021/mz400649w.
- [19] J. Park, S.-H. Yu, Y.-E. Sung, Design of structural and functional nanomaterials for lithium-sulfur batteries, Nano Today 18 (2018) 35–64. https://doi.org/10.1016/j.nantod.2017.12.010.
- [20] A.S.M. Ghumman, R. Shamsuddin, M.M. Nasef, W.Z.N. Yahya, A. Abbasi, H. Almohamadi, Sulfur enriched slow-release coated urea produced from inverse vulcanized copolymer, Sci. Total Environ. 846 (2022) 157417. https://doi.org/10.1016/j.scitotenv.2022.157417.
- [21] S.F. Valle, A.S. Giroto, C. Ribeiro, Unveiling the role of polysulfide matrices in phosphate diffusion for controlled release fertilizers, ACS Appl. Polym. Mater. 5 (2023) 6941–6949. https://doi.org/10.1021/acsapm.3c00988.
- [22] M. Mann, J.E. Kruger, F. Andari, J. McErlean, J.R. Gascooke, J.A. Smith, M.J.H. Worthington, C.C.C. McKinley, J.A. Campbell, D.A. Lewis, T. Hasell, M. V. Perkins, J.M. Chalker, Sulfur polymer composites as controlled-release fertilisers, Org. Biomol. Chem. 17 (2019) 1929–1936. https://doi.org/10.1039/C8OB02130A.
- [23] R.A. Dop, D.R. Neill, T. Hasell, Antibacterial activity of inverse vulcanized polymers, Biomacromolecules 22 (2021) 5223–5233. https://doi.org/10.1021/acs.biomac.1c01138.

- [24] R.A. Dop, D.R. Neill, T. Hasell, Sulfur-polymer nanoparticles: preparation and antibacterial activity, ACS Appl. Mater. Interfaces 15 (2023) 20822–20832. https://doi.org/10.1021/acsami.3c03826.
- [25] Z. Ren, X. Jiang, L. Liu, C. Yin, S. Wang, X. Yang, Modification of high sulfur polymer using a mixture porogen and its application as advanced adsorbents for Au(III) from wastewater, J. Mol. Liq. 328 (2021) 115437. https://doi.org/10.1016/j.molliq.2021.115437.
- [26] S. Petcher, D.J. Parker, T. Hasell, Macroporous sulfur polymers from a sodium chloride porogen—a low cost, versatile remediation material, Environ. Sci. Water Res. Technol. (2019) 2142–2149. https://doi.org/10.1039/C9EW00477G.
- [27] L.-A. Ko, Y.-S. Huang, Y.A. Lin, Bipyridine-containing polysulfide materials for broad-spectrum removal of heavy metals from water, ACS Appl. Polym. Mater. 3 (2021) 3363–3372. https://doi.org/10.1021/acsapm.1c00259.
- [28] N.A. Lundquist, M.J.H. Worthington, N. Adamson, C.T. Gibson, M.R. Johnston, A. V. Ellis, J.M. Chalker, Polysulfides made from re-purposed waste are sustainable materials for removing iron from water, RSC Adv. 8 (2018) 1232–1236. https://doi.org/10.1039/C7RA11999B.
- [29] A. Haro-Martínez, R. Arroyo-Carrasco, L. Galván, A. Sayago, A.A. Cuadri, J.E. Martín-Alfonso, Á. Trujillo-Reyes, F.G. Fermoso, J. Cubero-Cardoso, J. Urbano, Competitive and synergistic effects of metal adsorption in water remediation processes mediated by hybrid copolymers, Chem. Eng. J. 470 (2023) 143905. https://doi.org/10.1016/j.cej.2023.143905.
- [30] Mercury, World Health Organ. (2024). https://www.who.int/news-room/fact-sheets/detail/mercury-and-health (accessed November 6, 2025).
- [31] R.G. Pearson, Hard and soft acids and bases, J. Am. Chem. Soc. 85 (1963) 3533–3539. https://doi.org/10.1021/ja00905a001.
- [32] M.P. Crockett, A.M. Evans, M.J.H. Worthington, I.S. Albuquerque, A.D. Slattery, C.T. Gibson, J.A. Campbell, D.A. Lewis, G.J.L. Bernardes, J.M. Chalker, Sulfur-limonene polysulfide: A material synthesized entirely from industrial by-products and its use in removing toxic metals from water and soil, Angew. Chem. 128 (2016) 1746–1750. https://doi.org/10.1002/ange.201508708.
- [33] D.J. Parker, H.A. Jones, S. Petcher, L. Cervini, J.M. Griffin, R. Akhtar, T. Hasell, Low cost and renewable sulfur-polymers by inverse vulcanisation, and their potential for mercury capture, J. Mater. Chem. A 23 (2017) 11682–11692. https://doi.org/10.1039/c6ta09862b.

- [34] D.J. Parker, S.T. Chong, T. Hasell, Sustainable inverse-vulcanised sulfur polymers, RSC Adv. 8 (2018) 27892–27899. https://doi.org/10.1039/c8ra04446e.
- [35] A.M. Abraham, S.V. Kumar, S.M. Alhassan, Porous sulphur copolymer for gas-phase mercury removal and thermal insulation, Chem. Eng. J. 332 (2018) 1–7. https://doi.org/10.1016/j.cej.2017.09.069.
- [36] L.A. Limjuco, G.M. Nisola, K.J. Parohinog, K.N.G. Valdehuesa, S.P. Lee, H. Kim, W.J. Chung, Water-insoluble hydrophilic polysulfides as microfibrous composites towards highly effective and practical Hg2+ capture, Chem. Eng. J. 378 (2019) 122216. https://doi.org/10.1016/j.cej.2019.122216.
- [37] L.A. Limjuco, H.T. Fissaha, H. Kim, G.M. Nisola, W.J. Chung, Sulfur copolymerization with hydrophilic comonomers as polysulfides in microbeads for highly efficient Hg2+ removal from wastewater, ACS Appl. Polym. Mater. 2 (2020) 4677–4689. https://doi.org/10.1021/acsapm.0c00725.
- [38] A.S.M. Ghumman, R. Shamsuddin, Z.A. Alothman, A. Waheed, A.M. Aljuwayid, R. Sabir, A. Abbasi, A. Sami, Amine-decorated methacrylic acid-based inverse vulcanized polysulfide for effective mercury removal from wastewater, ACS Omega 9 (2024) 4831–4840. https://doi.org/10.1021/acsomega.3c08361.
- [39] Y. Chen, A. Yasin, Y. Zhang, X. Zan, Y. Liu, L. Zhang, Preparation and modification of biomass-based functional rubbers for removing mercury(II) from aqueous solution, Materials 13 (2020) 632. https://doi.org/10.3390/ma13030632.
- [40] A. Yasin, Y. Chen, Y. Liu, L. Zhang, X. Zan, Y. Zhang, Hyperbranched multiple polythioamides made from elemental sulfur for mercury adsorption, Polym. Chem. 11 (2020) 810–819. https://doi.org/10.1039/c9py01544b.
- [41] A.S.M. Ghumman, R. Shamsuddin, A. Abbasi, M. Ahmad, Y. Yoshida, A. Sami, H. Almohamadi, The predictive machine learning model of a hydrated inverse vulcanized copolymer for effective mercury sequestration from wastewater, Sci. Total Environ. 908 (2024) 168034. https://doi.org/10.1016/j.scitotenv.2023.168034.
- [42] Y. Ma, C. Shi, Q. Hong, J. Du, H. Zhang, X. Zheng, Z. Qu, X. Zhang, H. Xu, Harnessing graft copolymerization and inverse vulcanization to engineer sulfur-enriched copolymers for the selective uptake of heavy metals, Sep. Purif. Technol. 362 (2025) 131902. https://doi.org/10.1016/j.seppur.2025.131902.
- [43] R. Shamsuddin, A.S.M. Ghumman, R. Steven, A. Sami, S. Waqas, Z.N. Ahmad, Efficient mercury removal from wastewater via carbonized inverse vulcanized copolymers, ACS ES&T Water 5 (2025) 1499–1509. https://doi.org/10.1021/acsestwater.5c00030.

- [44] Y. Sun, Y. Sun, Z. Li, Y. Zheng, L. Zheng, J. Hu, Mercury adsorption study and DFT calculations of sulfur-containing biomass composites prepared by inverse vulcanization, Int. J. Biol. Macromol. 281 (2024) 135868. https://doi.org/10.1016/j.ijbiomac.2024.135868.
- [45] Y. Sun, C. Yang, Y. Fu, T. Guo, G. Yan, J. Hu, Sulfur-containing adsorbent made by inverse vulcanization of sulfur/oleylamine/potato starch for efficient removal of Hg(II) ions, J. Environ. Chem. Eng. 11 (2023) 109806. https://doi.org/10.1016/j.jece.2023.109806.
- [46] T. Tian, R. Hu, B.Z. Tang, Room temperature one-step conversion from elemental sulfur to functional polythioureas through catalyst-free multicomponent polymerizations, J. Am. Chem. Soc. 140 (2018) 6156–6163. https://pubs.acs.org/doi/10.1021/jacs.8b02886.
- [47] Q. Pan, Q. Hong, Y. Fan, X. Sun, W. Huang, N. Yan, Z. Qu, H. Xu, Efficient selective uptake of mercury ions using inverse vulcanization-synthesized sulfur-rich adsorbents, Sep. Purif. Technol. 333 (2024) 125917. https://doi.org/10.1016/j.seppur.2023.125917.
- [48] X. Wu, J.A. Smith, S. Petcher, B. Zhang, D.J. Parker, J.M. Griffin, T. Hasell, Catalytic inverse vulcanization, Nat. Commun. 10 (2019) 647. https://doi.org/10.1038/s41467-019-08430-8.
- [49] F.G. Müller, L.S. Lisboa, J.M. Chalker, Inverse vulcanized polymers for sustainable metal remediation, Adv. Sustain. Syst. 7 (2023) 2300010. https://doi.org/10.1002/adsu.202300010.
- [50] W. Sheard, K.W. Park, E.M. Leitao, Polysulfides as sorbents in support of sustainable recycling, ACS Sustain. Chem. Eng. 11 (2023) 3557–3567. https://doi.org/10.1021/acssuschemeng.2c07386.
- [51] A. Nayeem, M.F. Ali, J.H. Shariffuddin, The recent development of inverse vulcanized polysulfide as an alternative adsorbent for heavy metal removal in wastewater, Environ. Res. 216 (2023) 114306. https://doi.org/10.1016/j.envres.2022.114306.
- [52] J.M. Chalker, M. Mann, M.J.H. Worthington, L.J. Esdaile, Polymers made by inverse vulcanization for use as mercury sorbents, Org. Mater. 03 (2021) 362–373. https://doi.org/10.1055/a-1502-2611.
- [53] G. Li, S. Wang, Y. Zhang, M. Li, Z. Chen, J. Lu, Revisiting the role of polysulfides in lithium–sulfur batteries, Adv. Mater. 30 (2018) 1705590. https://doi.org/10.1002/adma.201705590.
- [54] F. Stojcevski, M.K. Stanfield, D.J. Hayne, M. Mann, N.A. Lundquist, J.M. Chalker, L.C. Henderson, Inverse vulcanisation of canola oil as a route to recyclable chopped carbon

- fibre composites, Sustain. Mater. Technol. 32 (2022) e00400. https://doi.org/10.1016/j.susmat.2022.e00400.
- [55] K. Orme, A.H. Fistrovich, C.L. Jenkins, Tailoring polysulfide properties through variations of inverse vulcanization, Macromolecules 53 (2020) 9353–9361. https://doi.org/10.1021/acs.macromol.0c01932.
- [56] J. Bao, K.P. Martin, E. Cho, K.-S. Kang, R.S. Glass, V. Coropceanu, J.-L. Bredas, W.O. Parker, J.T. Njardarson, J. Pyun, On the mechanism of the inverse vulcanization of elemental sulfur: Structural characterization of poly(sulfur- random -(1,3-diisopropenylbenzene)), J. Am. Chem. Soc. 145 (2023) 12386–12397. https://doi.org/10.1021/jacs.3c03604.
- [57] P. Yan, W. Zhao, F. McBride, D. Cai, J. Dale, V. Hanna, T. Hasell, Mechanochemical synthesis of inverse vulcanized polymers, Nat. Commun. 13 (2022) 4824. https://doi.org/10.1038/s41467-022-32344-7.
- [58] H. Hu, Y. Hu, H. Cheng, S. Dai, K. Song, M. Liu, Organic polysulfanes grafted on porous graphene as an electrode for high-performance lithium organosulfur batteries, J. Power Sources 491 (2021) 229617. https://doi.org/10.1016/j.jpowsour.2021.229617.
- [59] Y. Zhang, R.S. Glass, K. Char, J. Pyun, Recent advances in the polymerization of elemental sulphur, inverse vulcanization and methods to obtain functional Chalcogenide Hybrid Inorganic/Organic Polymers (CHIPs), Polym. Chem. 10 (2019) 4078–4105. https://doi.org/10.1039/C9PY00636B.
- [60] F. Zhao, Y. Li, W. Feng, Recent advances in applying vulcanization/inverse vulcanization methods to achieve high-performance sulfur-containing polymer cathode materials for Li–S batteries, Small Methods 2 (2018) 1800156. https://doi.org/10.1002/smtd.201800156.
- [61] I. Gomez, O. Leonet, J.A. Blazquez, D. Mecerreyes, Inverse vulcanization of sulfur using natural dienes as sustainable materials for lithium–sulfur batteries, ChemSusChem 9 (2016) 3419–3425. https://doi.org/10.1002/cssc.201601474.
- [62] J. Lim, J. Pyun, K. Char, Recent approaches for the direct use of elemental sulfur in the synthesis and processing of advanced materials, Angew. Chem. Int. Ed. 54 (2015) 3249–3258. https://doi.org/10.1002/anie.201409468.
- [63] J.J. Griebel, R.S. Glass, K. Char, J. Pyun, Polymerizations with elemental sulfur: A novel route to high sulfur content polymers for sustainability, energy and defense, Prog. Polym. Sci. 58 (2016) 90–125. https://doi.org/10.1016/j.progpolymsci.2016.04.003.
- [64] M.J.H. Worthington, R.L. Kucera, J.M. Chalker, Green chemistry and polymers made from sulfur, Green Chem. 19 (2017) 2748–2761. https://doi.org/10.1039/c7gc00014f.

- [65] H. Mutlu, E.B. Ceper, X. Li, J. Yang, W. Dong, M.M. Ozmen, P. Theato, Sulfur chemistry in polymer and materials science, Macromol. Rapid Commun. 40 (2019) 1800650. https://doi.org/10.1002/marc.201800650.
- [66] J.M. Chalker, M.J.H. Worthington, N.A. Lundquist, L.J. Esdaile, Synthesis and applications of polymers made by inverse vulcanization, Top. Curr. Chem. 377 (2019) 16. https://doi.org/10.1007/s41061-019-0242-7.
- [67] A. Abbasi, M.M. Nasef, W.Z.N. Yahya, Copolymerization of vegetable oils and bio-based monomers with elemental sulfur: A new promising route for bio-based polymers, Sustain. Chem. Pharm. 13 (2019) 100158. https://doi.org/10.1016/j.scp.2019.100158.
- [68] A.S.M. Ghumman, M.M. Nasef, M.R. Shamsuddin, A. Abbasi, Evaluation of properties of sulfur-based polymers obtained by inverse vulcanization: Techniques and challenges, Polym. Polym. Compos. 29 (2021) 1333–1352. https://doi.org/10.1177/0967391120954072.
- [69] A. Nayeem, M.F. Ali, J.H. Shariffuddin, Synthesis and applications of inverse vulcanized polysulfides from bio-crosslinkers, Mater. Today Proc. 57 (2022) 1095–1100. https://doi.org/10.1016/j.matpr.2021.09.397.
- [70] T. Lee, P.T. Dirlam, J.T. Njardarson, R.S. Glass, J. Pyun, Polymerizations with elemental sulfur: from petroleum refining to polymeric materials, J. Am. Chem. Soc. 144 (2022) 5–22. https://doi.org/10.1021/jacs.1c09329.
- [71] K.S. Kang, K.A. Iyer, J. Pyun, On the fundamental polymer chemistry of inverse vulcanization for statistical and segmented copolymers from elemental sulfur, Chem. Eur. J. 28 (2022) e202200115. https://doi.org/10.1002/chem.202200115.
- [72] P. Saini, N. Sandhu, A review on use of elemental sulphur in the synthesis of sulphurbased polymers, Mater. Today Proc. (2023). https://doi.org/10.1016/j.matpr.2023.03.047.
- [73] Y. Zhang, F. Seidi, M. Ahmad, L. Zheng, L. Cheng, Y. Huang, H. Xiao, Green and sustainable natural derived polysulfides for a broad range of applications, Green Chem. 25 (2023) 6515–6537. https://doi.org/10.1039/d3gc02005c.
- [74] S. Cherumukkil, S. Agrawal, R.V. Jasra, Sulfur polymer as emerging advanced materials: Synthesis and applications, ChemistrySelect 8 (2023) e202204428. https://doi.org/10.1002/slct.202204428.
- [75] R. Amna, S.M. Alhassan, A comprehensive exploration of polysulfides, from synthesis techniques to diverse applications and future frontiers, ACS Appl. Polym. Mater. 6 (2024) 4350–4377. https://doi.org/10.1021/acsapm.4c00272.
- [76] L.J. Dodd, Inverse vulcanisation: a new starter's guide to an emerging field, RSC Appl. Polym. 3 (2024) 10–42. https://doi.org/10.1039/d4lp00255e.

- [77] H. Shen, B. Zheng, H. Zhang, A decade development of inverse vulcanization towards green and sustainable practices, Polym. Rev. 64 (2024) 1211–1266. https://doi.org/10.1080/15583724.2024.2382891.
- [78] C.W. Schmitt, L.J. Dodd, J.K. Walz, L. Deterding, P. Lott, A.P. Grimm, M.P. Shaver, T. Hasell, P. Théato, A critical review on the sustainability of inverse vulcanised polymers, RSC Sustain. 3 (2025) 4190–4227. https://doi.org/10.1039/D5SU00387C.
- [79] A.W. Weitkamp, I. The action of sulfur on terpenes. The limonene sulfides, J. Am. Chem. Soc. 81 (1959) 3430–3434. https://doi.org/10.1021/ja01522a069.
- [80] A.W. Weitkamp, II. The action of raney nickel on limonene sulfides and sulfones, J. Am. Chem. Soc. 81 (1959) 3434–3437. https://doi.org/10.1021/ja01522a070.
- [81] A.W. Weitkamp, III. Mechanism of the formation of limonene sulfides, J. Am. Chem. Soc. 81 (1959) 3437–3439. https://doi.org/10.1021/ja01522a071.
- [82] R. Amna, K. Ali, S.M. Alhassan, Computational fluid dynamics analysis of mercury adsorption by inverse-vulcanized porous sulfur copolymers, Ind. Eng. Chem. Res. 62 (2023) 12277–12290. https://doi.org/10.1021/acs.iecr.3c01674.
- [83] T. Hasell, D.J. Parker, H.A. Jones, T. McAllister, S.M. Howdle, Porous inverse vulcanised polymers for mercury capture, Chem. Commun. 52 (2016) 5383–5386. https://doi.org/10.1039/c6cc00938g.
- [84] M.W. Thielke, L.A. Bultema, D.D. Brauer, B. Richter, M. Fischer, P. Theato, Rapid mercury(II) removal by electrospun sulfur copolymers, Polymers 8 (2016) 266. https://doi.org/10.3390/polym8070266.
- [85] J.S.M. Lee, D.J. Parker, A.I. Cooper, T. Hasell, High surface area sulfur-doped microporous carbons from inverse vulcanised polymers, J. Mater. Chem. A 35(2017) 18603–18609. https://doi.org/10.1039/c7ta07130b.
- [86] M.J.H. Worthington, R.L. Kucera, I.S. Albuquerque, C.T. Gibson, A. Sibley, A.D. Slattery, J.A. Campbell, S.F.K. Alboaiji, K.A. Muller, J. Young, N. Adamson, J.R. Gascooke, D. Jampaiah, Y.M. Sabri, S.K. Bhargava, S.J. Ippolito, D.A. Lewis, J.S. Quinton, A. V. Ellis, A. Johs, G.J.L. Bernardes, J.M. Chalker, Laying waste to mercury: inexpensive sorbents made from sulfur and recycled cooking oils, Chem. Eur. J. 23 (2017) 16219–16230. https://doi.org/10.1002/chem.201702871.
- [87] J. Lee, S. Lee, J. Kim, Z. Hanif, S. Han, S. Hong, M.H. Yoon, Solution-based sulfur-polymer coating on nanofibrillar films for immobilization of aqueous mercury ions, Bull. Korean Chem. Soc. 39 (2018) 84–89. https://doi.org/10.1002/bkcs.11350.

- [88] H.K. Lin, Y.S. Lai, Y.L. Liu, Cross-linkable and self-foaming polysulfide materials for repairable and mercury capture applications, ACS Sustain. Chem. Eng. 7 (2019) 4515–4522. https://doi.org/10.1021/acssuschemeng.8b06815.
- [89] S. Petcher, D.J. Parker, T. Hasell, Macroporous sulfur polymers from a sodium chloride porogen A low cost, versatile remediation material, Environ. Sci. Water Res. Technol. 5 (2019) 2142–2149. https://doi.org/10.1039/c9ew00477g.
- [90] A.D. Tikoalu, N.A. Lundquist, J.M. Chalker, Mercury sorbents made by inverse vulcanization of sustainable triglycerides: The plant oil structure influences the rate of mercury removal from water, Adv. Sustain. Syst. 4 (2020) 1900111. https://doi.org/10.1002/adsu.201900111.
- [91] V.S. Wadi, H. Mittal, E. Fosso-Kankeu, K.K. Jena, S.M. Alhassan, Mercury removal by porous sulfur copolymers: Adsorption isotherm and kinetics studies, Colloids Surf., A 606 (2020) 125333. https://doi.org/10.1016/j.colsurfa.2020.125333.
- [92] S. Petcher, B. Zhang, T. Hasell, Mesoporous knitted inverse vulcanised polymers, Chem. Commun. 57 (2021) 5059–5062. https://doi.org/10.1039/d1cc01152a.
- [93] B. Zhang, L.J. Dodd, P. Yan, T. Hasell, Mercury capture with an inverse vulcanized polymer formed from garlic oil, a bioderived comonomer, React. Funct. Polym. 161 (2021) 104865. https://doi.org/10.1016/j.reactfunctpolym.2021.104865.
- [94] B. Zhang, S. Petcher, H. Gao, P. Yan, D. Cai, G. Fleming, D.J. Parker, S.Y. Chong, T. Hasell, Magnetic sulfur-doped carbons for mercury adsorption, J. Colloid Interface Sci. 603 (2021) 728–737. https://doi.org/10.1016/j.jcis.2021.06.129.
- [95] Y. Fu, C. Yang, Y. Zheng, J. Jiang, Y. Sun, F. Chen, J. Hu, Sulfur crosslinked poly(m-aminothiophenol)/potato starch on mesoporous silica for efficient Hg(II) removal and reutilization of waste adsorbent as a catalyst, J. Mol. Liq. 328 (2021) 115420. https://doi.org/10.1016/j.molliq.2021.115420.
- [96] D. Cai, J.J. Dale, S. Petcher, X. Wu, T. Hasell, Investigating the effect of UV irradiation and TiO2 addition on heavy metal adsorption by inverse vulcanized sulfur polymers, Chem. Eur. J. (2024) e202402194. https://doi.org/10.1002/chem.202402194.
- [97] Y. Ma, C. Shi, J. Du, Z. Zhu, X. Zhang, Q. Wang, N. Liu, The key role of unsaturated olefin content on polysulfides prepared via inverse vulcanization of waste plant oils for mercury removal from wastewater, Environ. Sci. Pollut. Res. 31 (2024) 19753–19763. https://doi.org/10.1007/s11356-024-32452-5.
- [98] X. Deng, R.A. Dop, D. Cai, D.R. Neill, T. Hasell, Water-soluble ionic liquid-containing sulfur polymers for mercury capture, demulsification, and antibacterial activity, Adv. Funct. Mater. 34 (2024) 2311647. https://doi.org/10.1002/adfm.202311647.

- [99] N. Grassie, Recent work on the thermal degradation of acrylate and methacrylate homopolymers and copolymers, in: Chem. Transform. Polym., Butterworth & Co, 1972: pp. 119–134. https://doi.org/10.1016/B978-0-408-70310-9.50011-3.
- [100] M. Worzakowska, Thermal behavior, decomposition mechanism and some physicochemical properties of starch-g-poly(benzyl acrylate) copolymers, J. Therm. Anal. Calorim. 126 (2016) 531–540. https://doi.org/10.1007/s10973-016-5603-7.
- [101] N. Grassie, A. Scotney, R. Jenkins, T.I. Davis, Relationships between thermal, photothermal and photolytic degradation processes in methacrylate/acrylate copolymers, Chem. Zvesti. 26 (1972) 208–216. https://chempap.org/file_access.php?file=263a208.pdf (Accessed on November 6, 2025)
- [102] H. Wang, Q. Gao, J. Hu, High hydrogen storage capacity of porous carbons prepared by using activated carbon, J. Am. Chem. Soc. 131 (2009) 7016–7022. https://doi.org/10.1021/ja8083225.
- [103] F.A. Leibfarth, M. Wolffs, L.M. Campos, K. Delany, N. Treat, M.J. Kade, B. Moon, C.J. Hawker, Low-temperature ketene formation in materials chemistry through molecular engineering, Chem. Sci. 3 (2012) 766–771. https://doi.org/10.1039/C2SC00841F.
- [104] L. González, X. Ramis, J.M. Salla, A. Mantecón, A. Serra, Reduction of the shrinkage of thermosets by the cationic curing of mixtures of diglycidyl ether of bisphenol A and 6,6-dimethyl-(4,8-dioxaspiro[2.5]octane-5,7-dione), J. Polym. Sci., Part A: Polym. Chem. 44 (2006) 6869–6879. https://doi.org/10.1002/pola.21776.
- [105] S.J. García, J. Suay, Anticorrosive properties of an epoxy-Meldrum acid cured system catalyzed by erbium III trifluromethanesulfonate, Prog. Org. Coat. 57 (2006) 319–331. https://doi.org/10.1016/j.porgcoat.2006.09.011.
- [106] S.J. García, A. Serra, J. Suay, New powder coatings with low curing temperature and enhanced mechanical properties obtained from DGEBA epoxy resins and meldrum acid using erbium triflate as curing agent, J. Polym. Sci., Part A: Polym. Chem. 45 (2007) 2316–2327. https://doi.org/10.1002/pola.21998.
- [107] F.A. Leibfarth, Y. Schneider, N.A. Lynd, A. Schultz, B. Moon, E.J. Kramer, G.C. Bazan, C.J. Hawker, Ketene functionalized polyethylene: Control of cross-link density and material properties, J. Am. Chem. Soc. 132 (2010) 14706–14709. https://doi.org/10.1021/ja1060643.
- [108] F.A. Leibfarth, M. Kang, M. Ham, J. Kim, L.M. Campos, N. Gupta, B. Moon, C.J. Hawker, A facile route to ketene-functionalized polymers for general materials applications, Nat. Chem. 2 (2010) 207–212. https://doi.org/10.1038/nchem.538.

- [109] Y. Miyamura, C. Park, K. Kinbara, F.A. Leibfarth, C.J. Hawker, T. Aida, Controlling volume shrinkage in soft lithography through heat-induced cross-linking of patterned nanofibers, J. Am. Chem. Soc. 133 (2011) 2840–2843. https://doi.org/10.1021/ja110901h.
- [110] H. Jung, F.A. Leibfarth, S. Woo, S. Lee, M. Kang, B. Moon, C.J. Hawker, J. Bang, Efficient surface neutralization and enhanced substrate adhesion through ketene mediated crosslinking and functionalization, Adv. Funct. Mater. 23 (2013) 1597–1602. https://doi.org/10.1002/adfm.201201352.
- [111] L. González, F. Ferrando, X. Ramis, J.M. Salla, A. Mantecón, A. Serra, Characterization of new reworkable thermosetting coatings obtained by cationic and anionic curing of DGEBA and some Meldrum acid derivatives, Prog. Org. Coat. 65 (2009) 175–181. https://doi.org/10.1016/j.porgcoat.2008.10.007.
- [112] N.A. Lundquist, Y. Yin, M. Mann, S.J. Tonkin, A.D. Slattery, G.G. Andersson, C.T. Gibson, J.M. Chalker, Magnetic responsive composites made from a sulfur-rich polymer, Polym. Chem. 13 (2022) 5659–5665. https://doi.org/10.1039/D2PY00903J.
- [113] M. Mann, B. Zhang, S.J. Tonkin, C.T. Gibson, Z. Jia, T. Hasell, J.M. Chalker, Processes for coating surfaces with a copolymer made from sulfur and dicyclopentadiene, Polym. Chem. 13 (2022) 1320–1327. https://doi.org/10.1039/D1PY01416A.
- [114] M.J.H. Worthington, M. Mann, I.Y. Muhti, A.D. Tikoalu, C.T. Gibson, Z. Jia, A.D. Miller, J.M. Chalker, Modelling mercury sorption of a polysulfide coating made from sulfur and limonene, Phys. Chem. Chem. Phys. 24 (2022) 12363–12373. https://doi.org/10.1039/D2CP01903E.
- [115] EPA Water Filtration Manual, Environmental protection agency, 2020. https://www.epa.ie/publications/compliance--enforcement/drinking-water/advice--guidance/EPA-Water-Filtration-Manual.pdf (accessed November 6, 2025).
- [116] S. Jimenez-Falcao, A. Villalonga, J. Parra-Nieto, A. Llopis-Lorente, P. Martinez-Ruiz, R. Martinez-Mañez, R. Villalonga, Dithioacetal-mechanized mesoporous nanosensor for Hg(II) determination, Microporous Mesoporous Mater. 297 (2020) 110054. https://doi.org/10.1016/j.micromeso.2020.110054.
- [117] M.J. Park, G.M. Nisola, A.B. Beltran, R.E.C. Torrejos, J.G. Seo, S.-P. Lee, H. Kim, W.-J. Chung, Recyclable composite nanofiber adsorbent for Li+ recovery from seawater desalination retentate, Chem. Eng. J. 254 (2014) 73–81. https://doi.org/10.1016/j.cej.2014.05.095.
- [118] L.A. Limjuco, F.K. Burnea, Evaluation of dithiadiamide-based molecular ion imprinted polymer (MIIP) for selective recovery of platinum from acid-digested spent automobile catalytic converter (ACC) solution, MRS Commun. 12 (2022) 175–182. https://doi.org/10.1557/s43579-022-00158-9.

- [119] Natural Rubber Producers' Research Association, The Chemistry and physics of rubber-like substances: Studies of the Natural Rubber Producers' Research Association, Maclaren & Sons Ltd, London, 1963.
- [120] R. Hu, W. Li, B.Z. Tang, Recent advances in alkyne-based multicomponent polymerizations, Macromol. Chem. Phys. 217 (2016) 213–224. https://doi.org/10.1002/macp.201500291.
- [121] B. Wei, W. Li, Z. Zhao, A. Qin, R. Hu, B.Z. Tang, Metal-free multicomponent tandem polymerizations of alkynes, amines, and formaldehyde toward structure- and sequence-controlled luminescent polyheterocycles, J. Am. Chem. Soc. 139 (2017) 5075–5084. https://doi.org/10.1021/jacs.6b12767.
- [122] O. Kreye, T. Tóth, M.A.R. Meier, Introducing multicomponent reactions to polymer science: Passerini reactions of renewable monomers, J. Am. Chem. Soc. 133 (2011) 1790–1792. https://doi.org/10.1021/ja1113003.
- [123] X.-X. Deng, L. Li, Z.-L. Li, A. Lv, F.-S. Du, Z.-C. Li, Sequence regulated poly(esteramide)s based on Passerini reaction, ACS Macro Lett. 1 (2012) 1300–1303. https://doi.org/10.1021/mz300456p.
- [124] I.-H. Lee, H. Kim, T.-L. Choi, Cu-catalyzed multicomponent polymerization to synthesize a library of poly(N -sulfonylamidines), J. Am. Chem. Soc. 135 (2013) 3760–3763. https://doi.org/10.1021/ja312592e.
- [125] W. Li, X. Wu, Z. Zhao, A. Qin, R. Hu, B.Z. Tang, Catalyst-free, atom-economic, multicomponent polymerizations of aromatic diynes, elemental sulfur, and aliphatic diamines toward luminescent polythioamides, Macromolecules 48 (2015) 7747–7754. https://doi.org/10.1021/acs.macromol.5b02193.
- [126] T. Nguyen, L. Ermolenko, A. Al-Mourabit, Three-component reaction between isocyanides, aliphatic amines and elemental sulfur: Preparation of thioureas under mild conditions with complete atom economy, Synthesis 46 (2014) 3172–3179. https://doi.org/10.1055/s-0034-1379327.
- [127] T.B. Nguyen, M.Q. Tran, L. Ermolenko, A. Al-Mourabit, Three-component reaction between alkynes, elemental sulfur, and aliphatic amines: A general, straightforward, and atom economical approach to thioamides, Org. Lett. 16 (2014) 310–313. https://doi.org/10.1021/ol403345e.
- [128] K.-S. Kang, C. Olikagu, T. Lee, J. Bao, J. Molineux, L.N. Holmen, K.P. Martin, K.-J. Kim, K.H. Kim, J. Bang, V.K. Kumirov, R.S. Glass, R.A. Norwood, J.T. Njardarson, J. Pyun, Sulfenyl chlorides: An alternative monomer feedstock from elemental sulfur for polymer synthesis, J. Am. Chem. Soc. 144 (2022) 23044–23052. https://doi.org/10.1021/jacs.2c10317.

- [129] J.M.M. Pople, T.P. Nicholls, L.N. Pham, W.M. Bloch, L.S. Lisboa, M. V. Perkins, C.T. Gibson, M.L. Coote, Z. Jia, J.M. Chalker, Electrochemical synthesis of poly(trisulfides), J. Am. Chem. Soc. 145 (2023) 11798–11810. https://doi.org/10.1021/jacs.3c03239.
- [130] M. Mann, T.P. Nicholls, H.D. Patel, L.S. Lisboa, J.M.M. Pople, L.N. Pham, M.J.H. Worthington, M.R. Smith, Y. Yin, G.G. Andersson, C.T. Gibson, L.J. Esdaile, C.E. Lenehan, M.L. Coote, Z. Jia, J.M. Chalker, Sustainable gold extraction from ore and electronic waste, Nat. Sustain. 8 (2025) 947–956. https://doi.org/10.1038/s41893-025-01586-w.
- [131] J. Wang, X. Feng, C.W.N. Anderson, Y. Xing, L. Shang, Remediation of mercury contaminated sites A review, J. Hazard. Mater. 221–222 (2012) 1–18. https://doi.org/10.1016/j.jhazmat.2012.04.035.
- [132] W. Luo, G. Xiao, F. Tian, J.J. Richardson, Y. Wang, J. Zhou, J. Guo, X. Liao, B. Shi, Engineering robust metal—phenolic network membranes for uranium extraction from seawater, Energy Environ. Sci. 12 (2019) 607–614. https://doi.org/10.1039/C8EE01438H.
- [133] T.-H. Pham, B.-K. Lee, J. Kim, Improved adsorption properties of a nano zeolite adsorbent toward toxic nitrophenols, Process Saf. Environ. Prot. 104 (2016) 314–322. https://doi.org/10.1016/j.psep.2016.08.018.
- [134] S. Li, X. Huang, J. Liu, L. Lu, K. Peng, R. Bhattarai, PVA/PEI crosslinked electrospun nanofibers with embedded La(OH)3 nanorod for selective adsorption of high flux low concentration phosphorus, J. Hazard. Mater. 384 (2020) 121457. https://doi.org/10.1016/j.jhazmat.2019.121457.
- [135] R. Singh, M.K. Purkait, Microfiltration Membranes, in: Membr. Sep. Princ. Appl. From Material Selection to Mechanisms and Industrial, Elsevier, 2019: pp. 111–146. https://doi.org/10.1016/B978-0-12-812815-2.00004-1.
- [136] W. Zhao, Z. Zhang, Y. Xin, R. Xiao, F. Gao, H. Wu, W. Wang, Q. Guan, K. Lu, Na2S-modified biochar for Hg(II) removal from wastewater: A techno-economic assessment, Fuel 356 (2024) 129641. https://doi.org/10.1016/j.fuel.2023.129641.
- [137] M.I. El-Khaiary, Least-squares regression of adsorption equilibrium data: Comparing the options, J. Hazard. Mater. 158 (2008) 73–87. https://doi.org/10.1016/j.jhazmat.2008.01.052.
- [138] A. Malek, S. Farooq, Comparison of isotherm models for hydrocarbon adsorption on activated carbon, AIChE J. 42 (1996) 3191–3201. https://doi.org/10.1002/aic.690421120.

- [139] S. Ayoob, A.K. Gupta, Insights into isotherm making in the sorptive removal of fluoride from drinking water, J. Hazard. Mater. 152 (2008) 976–985. https://doi.org/10.1016/j.jhazmat.2007.07.072.
- [140] B. Boulinguiez, P. Le Cloirec, D. Wolbert, Revisiting the determination of langmuir parameters—Application to tetrahydrothiophene adsorption onto activated carbon, Langmuir 24 (2008) 6420–6424. https://doi.org/10.1021/la800725s.
- [141] R.D. Harter, Curve-fit errors in Langmuir adsorption maxima, Soil Sci. Soc. Am. J. 48 (1984) 749–752. https://doi.org/10.2136/sssaj1984.03615995004800040010x.
- [142] A. Jumasiah, T.G. Chuah, J. Gimbon, T.S.Y. Choong, I. Azni, Adsorption of basic dye onto palm kernel shell activated carbon: sorption equilibrium and kinetics studies, Desalination 186 (2005) 57–64. https://doi.org/10.1016/j.desal.2005.05.015.
- [143] K.V. Kumar, K. Porkodi, F. Rocha, Isotherms and thermodynamics by linear and non-linear regression analysis for the sorption of methylene blue onto activated carbon: Comparison of various error functions, J. Hazard. Mater. 151 (2008) 794–804. https://doi.org/10.1016/j.jhazmat.2007.06.056.
- [144] Y. Lai, G. Annadurai, F. Huang, J. Lee, Biosorption of Zn(II) on the different Ca-alginate beads from aqueous solution, Bioresour. Technol. 99 (2008) 6480–6487. https://doi.org/10.1016/j.biortech.2007.11.041.
- [145] P. Persoff, J.F. Thomas, Estimating Michaelis-Menten or Langmuir isotherm constants by weighted nonlinear least squares, Soil Sci. Soc. Am. J. 52 (1988) 886–889. https://doi.org/10.2136/sssaj1988.03615995005200030052x.
- [146] D. Ringot, B. Lerzy, K. Chaplain, J. Bonhoure, E. Auclair, Y. Larondelle, In vitro biosorption of ochratoxin A on the yeast industry by-products: Comparison of isotherm models, Bioresour. Technol. 98 (2007) 1812–1821. https://doi.org/10.1016/j.biortech.2006.06.015.
- [147] K.Y. Foo, B.H. Hameed, Insights into the modeling of adsorption isotherm systems, Chem. Eng. J. 156 (2010) 2–10. https://doi.org/10.1016/j.cej.2009.09.013.
- [148] K. Kumar, S. Sivanesan, Isotherm parameters for basic dyes onto activated carbon: Comparison of linear and non-linear method, J. Hazard. Mater. 129 (2006) 147–150. https://doi.org/10.1016/j.jhazmat.2005.08.022.
- [149] Y.C. Wong, Y.S. Szeto, W.H. Cheung, G. McKay, Adsorption of acid dyes on chitosan—equilibrium isotherm analyses, Process Biochem. 39 (2004) 695–704. https://doi.org/10.1016/S0032-9592(03)00152-3.

- [150] V.S. Mane, I.D. Mall, V.C. Srivastava, Use of bagasse fly ash as an adsorbent for the removal of brilliant green dye from aqueous solution, Dyes Pigm. 73 (2007) 269–278. https://doi.org/10.1016/j.dyepig.2005.12.006.
- [151] Y.S. Ho, J.F. Porter, G. McKay, Equilibrium isotherm studies for the sorption of divalent metal ions onto peat: Copper, Nickel and Lead single component systems, Water Air Soil Pollut. 141 (2002) 1–33. https://doi.org/10.1023/A:1021304828010.
- [152] S. Kundu, A.K. Gupta, Arsenic adsorption onto iron oxide-coated cement (IOCC): Regression analysis of equilibrium data with several isotherm models and their optimization, Chem. Eng. J. 122 (2006) 93–106. https://doi.org/10.1016/j.cej.2006.06.002.
- [153] C. Sabarinathan, P. Karuppasamy, C.T. Vijayakumar, T. Arumuganathan, Development of methylene blue removal methodology by adsorption using molecular polyoxometalate: Kinetics, thermodynamics and mechanistic study, Microchem. J. 146 (2019) 315–326. https://doi.org/10.1016/j.microc.2019.01.015.
- [154] A.A.A. Darwish, M. Rashad, H.A. AL-Aoh, Methyl orange adsorption comparison on nanoparticles: Isotherm, kinetics, and thermodynamic studies, Dyes Pigm. 160 (2019) 563–571. https://doi.org/10.1016/j.dyepig.2018.08.045.
- [155] N. Delgado, A. Capparelli, A. Navarro, D. Marino, Pharmaceutical emerging pollutants removal from water using powdered activated carbon: Study of kinetics and adsorption equilibrium, J. Environ. Manage. 236 (2019) 301–308. https://doi.org/10.1016/j.jenvman.2019.01.116.
- [156] Y. Shang, Y. Cui, R. Shi, P. Yang, J. Wang, Y. Wang, Regenerated WO2.72 nanowires with superb fast and selective adsorption for cationic dye: Kinetics, isotherm, thermodynamics, mechanism, J. Hazard. Mater. 379 (2019) 120834. https://doi.org/10.1016/j.jhazmat.2019.120834.
- [157] G. Ersan, Y. Kaya, M.S. Ersan, O.G. Apul, T. Karanfil, Adsorption kinetics and aggregation for three classes of carbonaceous adsorbents in the presence of natural organic matter, Chemosphere 229 (2019) 515–524. https://doi.org/10.1016/j.chemosphere.2019.05.014.
- [158] M. Hui, P. Shengyan, H. Yaqi, Z. Rongxin, Z. Anatoly, C. Wei, A highly efficient magnetic chitosan "fluid" adsorbent with a high capacity and fast adsorption kinetics for dyeing wastewater purification, Chem. Eng. J. 345 (2018) 556–565. https://doi.org/10.1016/j.cej.2018.03.115.
- [159] J. Wang, X. Guo, Adsorption kinetic models: Physical meanings, applications, and solving methods, J. Hazard. Mater. 390 (2020) 122156. https://doi.org/10.1016/j.jhazmat.2020.122156.

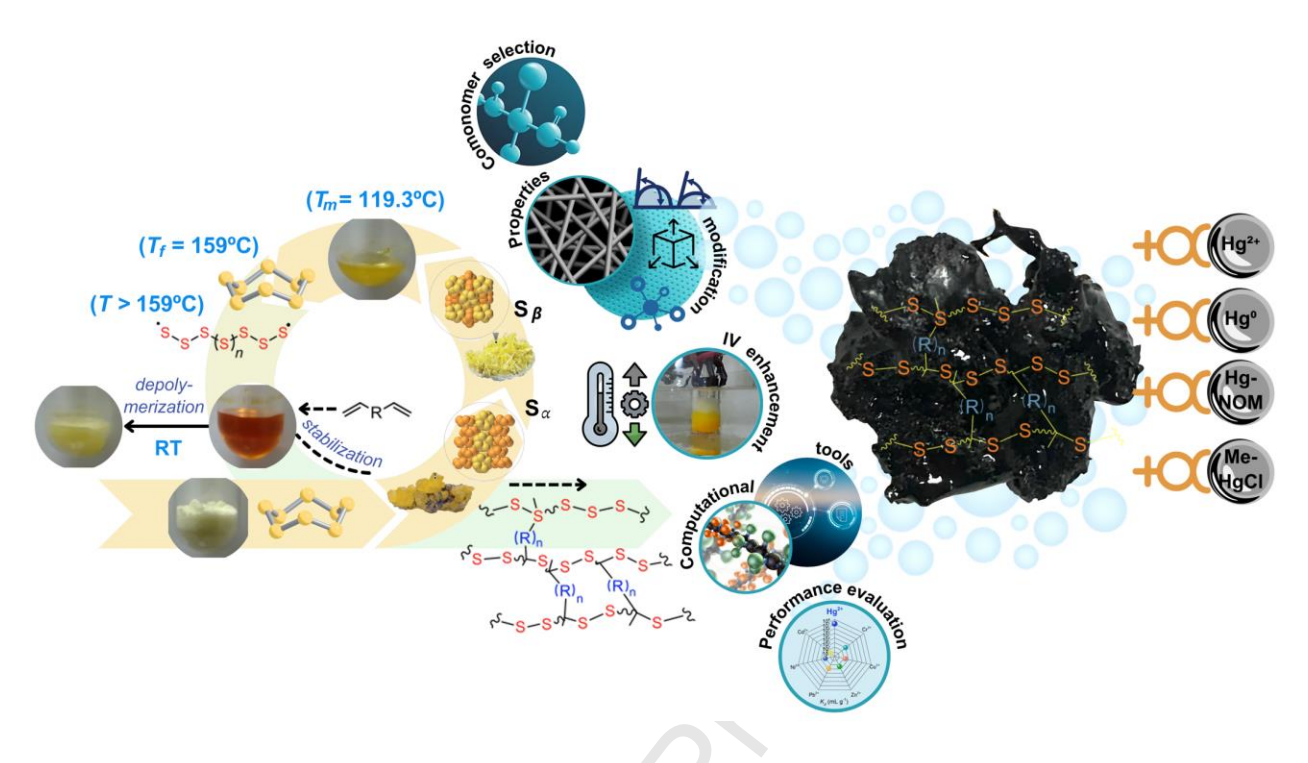
- [160] M.I. El-Khaiary, G.F. Malash, Y.-S. Ho, On the use of linearized pseudo-second-order kinetic equations for modeling adsorption systems, Desalination 257 (2010) 93–101. https://doi.org/10.1016/j.desal.2010.02.041.
- [161] K. Kumar, S. Sivanesan, Pseudo second order kinetics and pseudo isotherms for malachite green onto activated carbon: Comparison of linear and non-linear regression methods, J. Hazard. Mater. 136 (2006) 721–726. https://doi.org/10.1016/j.jhazmat.2006.01.003.
- [162] X. Guo, J. Wang, Comparison of linearization methods for modeling the Langmuir adsorption isotherm, J. Mol. Liq. 296 (2019) 111850. https://doi.org/10.1016/j.molliq.2019.111850.
- [163] Y. Ting, C. Chen, B.-L. Ch'ng, Y.-L. Wang, H.-C. Hsi, Using raw and sulfur-impregnated activated carbon as active cap for leaching inhibition of mercury and methylmercury from contaminated sediment, J. Hazard. Mater. 354 (2018) 116–124. https://doi.org/10.1016/j.jhazmat.2018.04.074.
- [164] U. Skyllberg, P.R. Bloom, J. Qian, C.-M. Lin, W.F. Bleam, Complexation of Mercury(II) in soil organic matter: EXAFS evidence for linear two-coordination with reduced sulfur groups, Environ. Sci. Technol. 40 (2006) 4174–4180. https://doi.org/10.1021/es0600577.
- [165] N. Sagawa, T. Shikata, Are all polar molecules hydrophilic? Hydration numbers of nitro compounds and nitriles in aqueous solution, Phys. Chem. Chem. Phys. 16 (2014) 13262–13270. https://doi.org/10.1039/C4CP01280A.
- [166] T. Shikata, M. Okuzono, Are all polar molecules hydrophilic? Hydration numbers of ketones and esters in aqueous solution, J. Phys. Chem. B 117 (2013) 7718–7723. https://doi.org/10.1021/jp4029968.
- [167] T. Shikata, M. Okuzono, N. Sugimoto, Temperature-dependent hydration/dehydration behavior of poly(ethylene oxide)s in aqueous solution, Macromolecules 46 (2013) 1956–1961. https://doi.org/10.1021/ma3026282.
- [168] T. Shikata, R. Takahashi, A. Sakamoto, Hydration of poly(ethylene oxide)s in aqueous solution as studied by dielectric relaxation measurements, J. Phys. Chem. B 110 (2006) 8941–8945. https://doi.org/10.1021/jp060356i.
- [169] T. Shikata, M. Okuzono, Hydration/dehydration behavior of polyalcoholic compounds governed by development of intramolecular hydrogen bonds, J. Phys. Chem. B 117 (2013) 2782–2788. https://doi.org/10.1021/jp400290b.
- [170] Y. Ono, T. Shikata, Contrary hydration behavior of N -isopropylacrylamide to its polymer, P(NIPAm), with a lower critical solution temperature, J. Phys. Chem. B 111 (2007) 1511–1513. https://doi.org/10.1021/jp068954k.

- [171] M.L. Eder, C.B. Call, C.L. Jenkins, Utilizing reclaimed petroleum waste to synthesize water-soluble polysulfides for selective heavy metal binding and detection, ACS Appl. Polym. Mater. 4 (2022) 1110–1116. https://doi.org/10.1021/acsapm.1c01536.
- [172] L. Guo, X. Xu, C. Niu, Q. Wang, J. Park, L. Zhou, H. Lei, X. Wang, X. Yuan, Machine learning-based prediction and experimental validation of heavy metal adsorption capacity of bentonite, Sci. Total Environ. 926 (2024) 171986. https://doi.org/10.1016/j.scitotenv.2024.171986.
- [173] W. Huo, Z. Zhu, H. Sun, B. Ma, L. Yang, Development of machine learning models for the prediction of the compressive strength of calcium-based geopolymers, J. Clean. Prod. 380 (2022) 135159. https://doi.org/10.1016/j.jclepro.2022.135159.
- [174] J. Qin, N. Gong, The estimation of the carbon dioxide emission and driving factors in China based on machine learning methods, Sustain. Prod. Consumption 33 (2022) 218–229. https://doi.org/10.1016/j.spc.2022.06.027.
- [175] I.B. Orhan, T.C. Le, R. Babarao, A.W. Thornton, Accelerating the prediction of CO2 capture at low partial pressures in metal-organic frameworks using new machine learning descriptors, Commun. Chem. 6 (2023) 214. https://doi.org/10.1038/s42004-023-01009-x.
- [176] A.O. Meray, S. Sturla, M.R. Siddiquee, R. Serata, S. Uhlemann, H. Gonzalez-Raymat, M. Denham, H. Upadhyay, L.E. Lagos, C. Eddy-Dilek, H.M. Wainwright, PyLEnM: A Machine Learning Framework for Long-Term Groundwater Contamination Monitoring Strategies, Environ. Sci. Technol. 56 (2022) 5973–5983. https://doi.org/10.1021/acs.est.1c07440.
- [177] X. Zhu, X. Wang, Y.S. Ok, The application of machine learning methods for prediction of metal sorption onto biochars, J. Hazard. Mater. 378 (2019) 120727. https://doi.org/10.1016/j.jhazmat.2019.06.004.
- [178] K.N. Palansooriya, J. Li, P.D. Dissanayake, M. Suvarna, L. Li, X. Yuan, B. Sarkar, D.C.W. Tsang, J. Rinklebe, X. Wang, Y.S. Ok, Prediction of soil heavy metal immobilization by biochar using machine learning, Environ. Sci. Technol. 56 (2022) 4187–4198. https://doi.org/10.1021/acs.est.1c08302.
- [179] V. Diniz, A. Mohamud, F.T. Rahman, H.T. Rana, N.A. Ogunwoolu, C.R. Crick, Inverse vulcanized sulfur polymers: A greener and cost-effective alternative to conventional polymers A cradle-to-gate life cycle analysis, J. Clean. Prod. 524 (2025) 146507. https://doi.org/10.1016/j.jclepro.2025.146507.
- [180] N.A.A. Qasem, R.H. Mohammed, D.U. Lawal, Removal of heavy metal ions from wastewater: a comprehensive and critical review, NPJ Clean Water 4 (2021) 36. https://doi.org/10.1038/s41545-021-00127-0.

Declaration of Interest Statement

△ The authors declare that they have no known competing financial interests or personal
relationships that could have appeared to influence the work reported in this paper.
☐ The author is an Editorial Board Member/Editor-in-Chief/Associate Editor/Guest Editor for
this journal and was not involved in the editorial review or the decision to publish this article.
\Box The authors declare the following financial interests/personal relationships which may be
considered as potential competing interests:

Graphical Abstract



Highlights

- Inverse vulcanized polysulfides emerge as green, low-cost Hg²⁺ adsorbents.
- Comonomer design tunes IV PS morphology, wettability, and adsorption sites.
- Normalized Hg²⁺ adsorption metrics are critical for fair performance evaluation.
- Digital tools (e.g., Machine learning and CFD) accelerate IV PS design and process optimization.
- Life cycle assessment validates the sustainability of IV PS for Hg remediation.